American Mineralogist, Volume 98, pages 1943–1965, 2013

What Lurks in the Martian Rocks and Soil? Investigations of Sulfates, Phosphates, and Perchlorates

Mössbauer parameters of iron in sulfate minerals†

M. Darby Dyar[1,*], Elly Breves[1], Erica Jawin[1,‡], Gerard Marchand[1], Melissa Nelms[1], Vanessa O'Connor[2], Samantha Peel[1,§], Yarrow Rothstein[1], Elizabeth C. Sklute[1,||], Melissa D. Lane[3], Janice L. Bishop[4] and Stanley A. Mertzman[5]

[1]Department of Astronomy, Mount Holyoke College, South Hadley, Massachusetts 01075, U.S.A.
[2]Department of Geosciences, Smith College, Northampton, Massachusetts 01063 , U.S.A.
[3]Planetary Science Institute, Tucson, Arizona 85719, U.S.A.
[4]SETI Institute/NASA-Ames Research Center, Mountain View, California, 94043, U.S.A.
[5]Department of Earth and Environment, Franklin and Marshall College, Lancaster, Pennsylvania 17603, U.S.A.

Abstract

Although Fe-sulfate minerals occur only rarely on Earth as alteration products of sulfidic basalts or in hydrothermal systems, multiple lines of evidence point to the importance of Fe- (and other) sulfate minerals on the surface of Mars. One such martian data set comes from the MIMOS II Mössbauer spectrometers on the Mars Exploration Rovers, which acquired hundreds of spectra from the martian surface at two locations. Interpretation of those spectra has been limited by the lack of a comprehensive set of laboratory analog spectra of the broad range of naturally occurring sulfate minerals. Accordingly, this study reports Mössbauer data of 98 samples representing 47 different sulfate mineral species, all containing six- or higher-coordinated Fe. The resultant Mössbauer parameters are related to the local polyhedral environment around the Fe cation in each mineral to explain variations in spectral characteristics. Results show that the size of the coordination polyhedron is the best predictor of quadrupole splitting, which increases with both octahedral volume and mean bond length. Species within groups of structurally similar minerals are shown to have comparable spectral peaks that generally fall within small ranges. Although coordination polyhedron geometry is not necessarily unique to any particular mineral species or group, Mössbauer data can be used to help constrain mineral identifications from martian spectra. The number of mineral species is large, but the range of crystal structures and hyperfine parameters may be small, so that in many cases, individual minerals cannot be uniquely fingerprinted. Examples would include quenstedtite, coquimbite, kornelite, and lausenite, which have indistinguishable spectra, as do apjohnite, bilinite, dietrichite, and römerite. Overlap of Mössbauer parameters is a particular complication for identification of Fe^{3+}-rich phases because the range of Mössbauer parameters for Fe^{3+} in any coordination number is so small. Previous analyses of martian Mössbauer spectra reported the presence of jarosite (Klingelhöfer et al. 2004; Morris et al. 2004) and an unspecific ferric sulfate (Morris et al. 2008). New data presented here indicate that botryogen, metasideronatrite, and slavikite exhibit Mössbauer spectra similar to those attributed to jarosite at Meridiani Planum. Fibroferrite and rhomboclase have parameters similar to those observed at Arad Samra, and copiapite and parabutlerite could be present at Tyrone Mount Darwin and Berkner Island. Unique mineral identifications are generally not possible from Mössbauer data alone, particularly for paramagnetic phases, although combining Mössbauer results with other data sets enables a greater level of confidence in constraining mineralogy. This study provides a new expansive data set for future interpretation of iron sulfates on Mars.

Keywords: Mössbauer, sulfate, jarosite, Mars

Introduction

Iron sulfates, many of which form as alteration products of sulfides, are relatively rare on Earth, particularly as hydrous species. They may form as a result of chemical interaction of acidic groundwater with mafic rocks (basalts) under ambient (and cold) conditions or in hydrothermal systems (Tosca et al. 2004). However, elsewhere in our Solar System, sulfur may be a more common and significant element in crustal rocks and thus conditions may be more favorable for the formation of sulfate minerals. This is especially true on Mars, where the low temperatures and pH found in the martian permafrost create ideal conditions for the formation of this group of minerals (Burns 1987), which includes such phases as coquimbite,

* E-mail: mdyar@mtholyoke.eud
‡ Present address: Department of Geological Sciences, Brown University, Providence, Rhode Island 02912, U.S.A.
§ Present address: Department of Earth and Planetary Science, University of Tennessee, Knoxville, Tennessee 37996, U.S.A.
|| Present address: Department of Geosciences, Stony Brook University, Stony Brook, New York 11794, U.S.A.

† Papers from 2012 AGU session: Sulfates, phosphates, and perchlorates have been found on Mars from orbit and/or from surface missions. Special Collection Associate Editors: Darby Dyar, Melissa Lane, and Janice Bishop. The GSW site (http://ammin.geoscienceworld.org/site/misc/specialissuelist.xhtml) has complete information.

0003-004X/13/1112–1943$05.00/DOI: http://dx.doi.org/10.2138/am.2013.4604

$Fe_2^{3+}(SO_4)_3 \cdot 9H_2O$, and amarantite, $FeSO_4(OH) \cdot 3H_2O$. Viking, Mars Pathfinder, Mars Exploration Rover, and remotely sensed data (e.g., Clark et al. 1982; Blaney and McCord 1995; Rieder et al. 2004; Bonello et al. 2004; McAdam et al. 2013; Yen et al. 2013) have all suggested that sulfur is a relatively abundant element on the surface of Mars, but the mineralogy of the sulfur-rich phases is not well constrained. Lane et al. (2004) suggests that hydrous iron sulfates (HIS) might contribute to the martian thermal emission, reflectance, and Mössbauer spectra.

Before the Mars Science Laboratory landed its CheMin instrument (Blake et al. 2012), the most pivotal tool for in situ identification of sulfate mineralogy on Mars was the MIMOS II Mössbauer spectrometer, which was part of the payload of both the Spirit and Opportunity rovers. Klingelhöfer et al. (2004) identified jarosite at Meridiani Planum, Mars, based on an isomer shift of 0.37 ± 0.02 mm/s and quadrupole splitting of 1.20 ± 0.02 mm/s. These Mössbauer parameters are the best match with jarosite of all the samples in the Mössbauer Effect Data Center database of published spectra and at that time there were no "reasonable alternatives for jarosite" (Morris et al. 2006). They further noted that the "jarosite" doublet seen in the Mars spectra was a perfect match to those previously reported for jarosite by Leclerc (1980). Moreover, the existence of jarosite and other sulfates had been predicted by Roger Burns in several papers (Burns 1986, 1987, 1988, 1993; Burns and Fisher 1990). For these reasons, the idea of jarosite on Mars became generally accepted, and has been commonly used to constrain phase equilibria and aqueous processes on Mars (Tosca et al. 2004).

This exciting report of iron sulfate on Mars (Klingelhöfer et al. 2004; Morris et al. 2006), along with subsequent discovery of an unspecific ferric sulfate (Morris et al. 2008), illuminated the need for further Mössbauer data on this important class of minerals. At that time, little was known about the Mössbauer parameters that are characteristic of related sulfate minerals. Only a handful of sulfate Mössbauer spectra had been reported in 2004 (mostly those of jarosite), and nearly all were acquired at room temperature, and thus not optimal for matching with ~220 K spectra from Mars. In subsequent years, several new studies have sought to characterize sulfate minerals (e.g., Majzlan et al. 2011; Van Alboom et al. 2009; Kovács et al. 2008; Ertl et al. 2008; Hyde et al. 2011), but most focused only on a few examples of a single mineral group. There remained a need for a robust survey of iron sulfate minerals acquired under consistent conditions, which is fulfilled by the current paper. These new data are expected to lead to new discoveries about iron sulfate minerals on Mars.

To address this deficiency, this study reports Mössbauer data of 98 samples representing 45 different sulfate mineral species. To put the data in a crystal chemical context, this paper seeks to relate the resultant Mössbauer parameters to both the local polyhedral environment around the Fe cations in these minerals and the overall structural characteristics of each species. The groundwork for these comparisons has been laid by the thorough discussion and classification of sulfate minerals presented by Hawthorne et al. (2000). It seems logical to assume that minerals of the same structure classes will have similar spectral features. Similarly, mineral species that belong to the same hydration sequence might also be assumed to have similar spectra. However, little work has been done to explore or test these hypotheses. This project was designed to look at the big picture and examine general trends in Mössbauer spectroscopy of sulfate minerals at 295 K. Mars's temperature measurements will be considered in a future paper.

Background

There are ~370 sulfate mineral species, and structures are known for about 80% of them (Hawthorne et al. 2000). Sulfates are similar to silicates (and phosphates and arsenates) in that the structures are based on a tetrahedral unit, SO_4, that is analogous to the familiar SiO_4 building blocks of most silicates. However, the charge of the S^{6+} cation is greater than that of Si^{4+}, so the O^{2-} anions in the SO_4^{2-} tetrahedra must be linked to satisfy charge balance in a manner that is different from what is observed in SiO_4^{4-}-based silicates.

For example, framework silicates such as quartz and feldspar are the most common minerals in the Earth's crust. They are based upon corner-sharing tetrahedra in which charge balance is satisfied by sharing all four corners of SiO_4^{4-} tetrahedra (with substitution of Al for Si accommodated by Na, Ca, and K in the case of feldspars). In the sulfate minerals, the structures are fundamentally different because this type of complete polymerization among solely SO_4^{2-} tetrahedra (or in combination with other tetrahedral oxyanions such as PO_4, AsO_4, VO_4, SiO_4) is unstable (Hawthorne et al. 2000). Another distinction of sulfate minerals is that substitution of other cations for S^{6+} is not as common, although it does occur in gypsum and beudantite ($As^{5+} \leftrightarrow S^{6+}$; Lin et al. 2013; Szymanski 1988) vergasvaite ($Mo^{6+} \leftrightarrow S^{6+}$; Berlepsch et al. 1999), and hashemite ($Cr^{6+} \leftrightarrow S^{6+}$; Duesler and Foord 1986). It is questionable whether $Fe^{3+} \leftrightarrow S^{6+}$ substitution even occurs because there are (to date) no Mössbauer studies that report tetrahedral Fe^{3+} in a sulfate mineral species. It is thus expected that Fe^{3+} in sulfate minerals will be generally confined to six-coordinated sites, which may also be occupied by Fe^{2+}. However, this study will examine the validity of this assumption.

So sulfate structures are commonly composed of SO_4^{2-} tetrahedra bonded with cations in octahedral (the vast majority) or larger coordination polyhedra (Fig. 1). Thus tetrahedral Fe^{3+} occupancy (i.e., in S-deficient structures) is highly unlikely. Interpretation of the Mössbauer spectra of these structures is greatly simplified, and is generally a matter of distinguishing between octahedral Fe^{3+} and Fe^{2+} (and rarely dodecahedral, as when Fe^{2+} might substitute into dodecahedral or larger sites in Ca sulfates such as anhydrite). These distinctions are described using the positions of the peaks in doublets of a Mössbauer spectrum using the terms isomer shift (IS, δ, or sometimes center shift) and quadrupole splitting (QS, ΔE_Q, or Δ), expressed in velocity units by convention in this field. Isomer shift is caused by overlap between the nucleus and the *s*-electron charge distributions that causes a shift in the nuclear energy levels in the Fe atom. Isomer shift is most sensitive to oxidation state and less sensitive to distortions in the surrounding site geometry. Isomer shift is measured as the offset of the doublet's centroid from zero velocity, and its value in silicates is generally low (0.25–0.5 mm/s) for octahedral Fe^{3+} and much higher (>1.10 mm/s) for octahedral Fe^{2+}. Its error is usually given as ±0.02 mm/s (Dyar 1984; Dyar et al. 2008).

Quadrupole splitting results from interactions between the

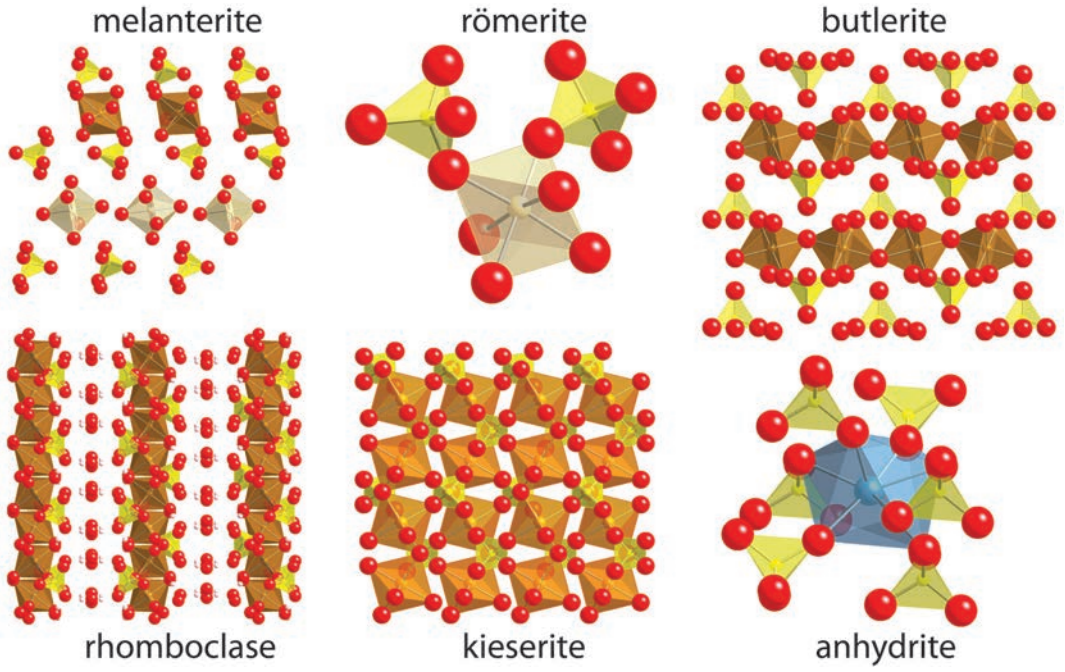

FIGURE 1. Contrasting structures within the sulfate minerals that combine SO_4 tetrahedra and $M(O,OH,OH_2)_6$ octahedra in various ways (Hawthorne et al. 2000): melanterite (structure from Peterson et al. 2003) has unconnected groups of SO_4 tetrahedra, römerite (Fanfani et al. 1970) has SO_4 tetrahedra linked to Fe2 octahedra in a *cis* arrangement on adjacent corners, butlerite (Fanfani et al. 1971) has infinite chains, rhomboclase (Mereiter 1974) has infinite sheets, and kieserite (Bregeault et al. 1970) has an infinite framework. Anhydrite (Hawthorne and Ferguson 1975) has a structure with SO_4 tetrahedra linked to larger cation sites that can accommodate Ca. (Color online.)

nuclear quadrupole moment and the gradient of the surrounding electric field, which cause the I = 3/2 level to split into two sublevels. QS is the separation between the two component peaks. QS is sensitive to both oxidation state and site geometry. As an example, consider Fe^{2+} in perfectly octahedral (sixfold) coordination. The electronic configuration of Fe^{2+}, $3d^6$, is in general high spin for minerals, i.e., $t_{2g}^4 e_g^2$. The sixth electron populates the three degenerate (all the same energy) t_{2g} levels equally, so spherical symmetry is maintained and, ignoring lattice terms, there is no quadrupole splitting. However, a distortion of the octahedral environment lifts the degeneracy of the t_{2g} levels, leading to unequal occupancy of the *d* orbitals and a large contribution to Δ from the electronic field. In high-spin Fe^{3+}, which has electronic configuration $t_{2g}^3 e_g^2$, the *d* orbitals remain equally populated even when the octahedral environment is distorted, and the electronic field remains spherical. Of course, in both cases, asymmetry in the lattice field causes $^{[6]}Fe^{2+}$ and $^{[6]}Fe^{3+}$ to split the I = 3/2 level, but usually, Δ for Fe^{2+} (>1.5 mm/s) >> Δ for Fe^{3+} (<1.3 mm/s). In general, the larger the Δ value, the more distorted the coordination polyhedron surrounding the Fe atom (Burns and Solberg 1990; Dyar et al. 2006a). The error of Δ on fitted spectra is usually given as ±0.02 mm/s (Dyar 1984; Dyar et al. 2008).

Given that the parameters have wide ranges, it may be possible to assign certain ranges of parameters to particular types of bonding environments or coordination polyhedra. Thus this paper presents Mössbauer spectra of well-characterized sulfate minerals and determines characteristic parameters for minerals with different structure types. In many cases, these are the first Mössbauer measurements of Fe^{3+}/Fe^{2+} ratios for these mineral species. The results shed light on stoichiometry and charge-balancing substitutions in these phases as well as the parageneses and redox environments in which these mineral form.

EXPERIMENTAL AND ANALYTICAL METHODS

Samples for this project (Table 1) were selected from the collections of the coauthors; others were purchased from collectors or came from E. Cloutis (U. Winnepeg), the National Museum of Natural History (Smithsonian) and the Harvard Mineralogical Museum. Diversity of samples from multiple localities was sought so that compositional variability within each group could be assessed. All samples were kept in dry air in a desiccator when not being analyzed. Samples were first handpicked to purify them, a step that was critical because many of these phases occur as intergrowths with other minerals. This job was made more difficult by the fact that many sulfates are yellow in color, making it necessary to distinguish coexisting phases on the bases of morphology and subtle color variations. However, it is important to note that in some cases, individual species were mingled with other species at such a small scale that it is unrealistic to expect that pure separates could be created. In such cases, minor contributions in spectra from the impurities would be expected. One of the advantages of the current study is that more than one example of most species was analyzed, and so the diagnostic spectral characteristics that various samples have in common can be identified despite the presence of potential impurities.

A majority of the separates was then analyzed by XRD to confirm their purity and make unequivocal phase identifications. This task was potentially complicated by the fact that several of these minerals are extremely rare, and thus not represented in XRD databases (e.g., ilesite and bilinite). For this reason, it was sometimes necessary in a few instances to make educated guesses about the identity of some minerals, drawing on the fact that many of the samples studied here came from their type localities. Each of these is detailed in the footnotes to Table 1. During the drawn-out collection and culling phase of the samples, various XRD analyses were conducted at Franklin and Marshall College, Smith College, Indiana University, and the University of New Mexico.

Samples were then prepared by mixing the sulfates with sucrose, gently

Table 1. Samples studied

Dana number	Mineral species	Locality	Sample number
28.3.1.2	Celestine	Maybee, MI	ML-S13
28.3.2.1	Anhydrite	Lavender Pit, Bisbee, Cochise Co., AZ	159266
28.3.2.1	Anhydrite	Borate, San Bernardino Co., CA	SPT132[1]
28.4.3.1	Yavapaiite	synthetic sample, courtesy Ferren Forray	ML-S79
29.1.1.1	Rhomboclase	Cerre de Pasco, Peru	81268
29.1.1.1	Rhomboclase	Alcaparra, Chile	ML-S85
29.1.1.1	Rhomboclase	Alcaparra, Chile	ML-S89
29.1.1.1	Rhomboclase	Near Cerritos Bay, Alcaparrosa, Chile	ML-S84
29.4.4.1	Ferrinatrite	Sierra Gorda, Cahacoles, Chile	R6214
29.4.4.1	Ferrinatrite	Sierra Gorda, Antofagaste, Chile	VZO105/106
29.4.6.1	Metavoltine	Mina Alcaparrosa, Calama, Atacama Desert, Chile	G2677
29.4.6.1	Metavoltine	Cetine Mine, Siena, Tuscany, Italy	VZO114[2]
29.5.1.1	Krausite	Sulfur Hole, Mule Canyon, San Bernard, CA	156916[3]
29.5.2.1	Goldichite	Pozzuoli, Solfatara (1969), Italy	123922
29.5.3.2	Amarantite	Los Pintados, Chile	G3775[4]
29.6.10.1	Melanterite	Locality unknown; Mount Holyoke College collection; sample labeled as boothite (Cu-melanterite)	2070[4]
29.6.2.2	Szomolnokite	Island Mountain, Trinity Co., CA	92942
29.6.2.2	Szomolnokite	Tintic Standard Mine, Dividend, UT	104276
29.6.2.2	Szomolnokite	Cuprian sample, Alma Pyrite mine, Alameda Co., CA	156925
29.6.2.2	Szomolnokite	Lavender Pit, Bisbee, Cochise Co., AZ	159266[5]
29.6.2.2	Szomolnokite	Rio Tinto Mine, Hvelva, Spain	136685-2
29.6.2.2	Szomolnokite	Joe Bishop Mine, San Juan Co., UT	ML-S103
29.6.2.2	Szomolnokite	Markey Mine, Red Canyon, San Juan Co., UT	ML-S60
29.6.2.2	Szomolnokite	Orovile, WA	ML-S77
29.6.2.3	Szmikite	Toyoha Mine, Sapporo, Ishikari, Hokkaido, Japan	159189[6]
29.6.2.5	Gunningite	Alma Pyrite Mine, Alameda Co., CA	156925
29.6.6.1	Rozenite	Island Mountain, Trinity Co., CA	JB626B
29.6.6.1	Rozenite	Oage Mine, Ominato, Aomori-ken, Honshu, Japan	SPT130
29.6.6.2	Starkeyite	Habachtal, Pinzgau, Salzburg, Austria	137725
29.6.6.2	Starkeyite	Veneables Valley, Basque, British Columbia, Canada	ML-S65
29.6.6.3	Ilesite	McDonnell Mine, Park Co., CO	123277[7]
29.6.7.1	Chalcanthite	Smolnik, Eastern Slovakia, Slovak Republic	DD100 green
29.6.7.3	Pentahydrite	2700 Level, Cambell Shaft, Bisbee, AZ	VZO121[8]
29.6.7.4	Jokokuite	Locality unknown; Mount Holyoke College collection	G3536[4]
29.7.2.1	Römerite	Island Mountain, Trinity Co., CA	93825
29.7.2.1	Römerite	Cerre de Pusco, Peru	113733
29.7.2.1	Römerite	Alcaparrosa, Chile	159098-2[9]
29.7.2.1	Römerite	near Skauriatissa, Island of Cyprus, Greece	R8415
29.7.2.1	Römerite	Sulphur Hole, near Borate, San Bernardino Co., CA	SPT110
29.7.2.1	Römerite	Alcaparrosa, Chile	SPT122/126
29.7.3.2	Halotrichite	The Geysers, Sonoma Co., CA	104135[10]
29.7.3.2	Halotrichite	Golden Queen Mine, Soledad Mountain, Kern Co., CA	G1616[4]
29.7.3.2	Halotrichite	Sulfur Hole Prospect, near Yermo, CA	VZO128
29.7.3.3	Apjohnite	Alum Cave, Sevier Co., TN	121356[4]
29.7.3.4	Dietrichite	unknown	G-2429[4]
29.7.3.5	Bilinite	Arco, ID	169017[11]
29.8.1.1	Lausenite	United Verde Mine, Jerome, AZ	102923

Notes: [1] Sample has minor coquimbite impurity. [2] Sample has a known Fe^{2+} römerite impurity. [3] XRD reports that this sample is geigerite but the locality is consistent with metavoltine. [4] No XRD; sample too small. [5] XRD of this sample suggests it is anhydrite but its parameters are an exact match to those of szomolnokite, which may be an impurity in the sample. [6] XRD suggests this sample is a complex solid solution between kieserite and szimikite. [7] XRD identification on this sample was spangolite, but ilesite is not correctly represented in the XRD database. Note that this sample comes from the Smithsonian and is from the ilesite type locality. [8] Minor impurities from pickeringite, starkeyite, botryogen, and boussingaultite. [9] No XRD on this sample but NMNH identification was römerite. [10] XRD found small copiapite contaminant. [11] XRD suggests alunogen and wupatkiite in this sample but bilinite is not represented in XRD database, and so NMNH ID is used here.

Table continued next page

mixing them into a homogeneous powder to fill the sample holder for Mössbauer spectroscopy. Then 295 K Mössbauer spectra were acquired using a source of 100–40 mCi ^{57}Co in Rh, which was used on a WEB Research Co. (now See Co.) model W100 spectrometer. Run times ranged from 12–96 h, and results were calibrated against α-Fe foil.

Spectra were fit with Lorentzian doublets using the MEX_FielDD program acquired from the University of Ghent courtesy of E. De Grave. Isomer shifts (IS or δ), and quadrupole splittings (QS or Δ) of the doublets were allowed to vary, and widths (full-width at half maximum) of all peaks were coupled to vary in pairs. All major Fe species were represented by well-resolved quadrupole pairs so the fits were straightforward, although it was sometimes necessary to fit small doublets representing impurities (Table 2[1]).

[1] Deposit item AM-13-1110, Table 2. Deposit items are available two ways: For a paper copy contact the Business Office of the Mineralogical Society of America (see inside front cover of recent issue for price information). For an electronic copy visit the MSA web site at http://www.minsocam.org, go to The American Mineralogist Contents, find the table of contents for the specific volume/issue wanted, and then click on the deposit link there.

Results: Mössbauer parameters

Mössbauer parameters for all samples studied at room temperature are given in full in Table 2 and for all doublets with areas >5% of the total peak area in Tables 3–6, where minerals with similar parameters are grouped together to compare and contrast features. Because Fe^{3+} and Fe^{2+} have quite distinct parameters, it is convenient to discuss the results and spectral features separately, beginning with the Fe^{3+}-bearing sulfates, which are the most numerous.

One of the most striking things about the data set for Fe^{3+} parameters is the consistency of the isomer shift (δ), which ranges from 0.37–0.52 mm/s, but is most commonly in the range from 0.41–0.43 mm/s (Fig. 2). Error bars associated with isomer shift are commonly quoted as ±0.01–0.05 mm/s, so many of the isomer shift values for Fe^{3+} sulfates are essentially the same.

TABLE 1.—*CONTINUED*

Dana number	Mineral species	Locality	Sample number
29.8.2.1	Kornelite	Smolnik, Slovenko, Czechoslavakia	95830[1]
29.8.3.1	Coquimbite	Borate, Calton Hills, San Bernardino, CA	R7661
29.8.3.1	Coquimbite	Atacama, Chile	ML-S63
29.8.3.1	Coquimbite	Dexter no.7 Mine, San Rafael Swell, UT	SPT119
29.8.3.1	Coquimbite	Alcaparrosa, Chile	SPT126
29.8.3.1	Coquimbite	Borate, San Bernardino Co., CA	SPT131
29.8.3.1	Coquimbite	Borate, San Bernardino County, CA	SPT132
29.8.3.1	Coquimbite	Helper, Carbon Co., UT	VZO101/102
29.8.5.1	Quensdedtite	Tierra Amarilla, Copiapo, Chile	B8255[2]
29.9.1.1	Voltaite	Jerome District, AZ	85679
29.9.1.1	Voltaite	Smolnik, eastern Slovakia, Slovak Republic	95830
29.9.1.1	Voltaite	United Verde Mine, Jerome, AZ	115035
29.9.1.1	Voltaite	Boron Kern Country, CA	129313
29.9.1.1	Voltaite	Boron Kern Country, CA	137958
29.9.1.1	Voltaite	Minas Rio Tinto, Hvelva, Andalucia, Spain	158795
29.9.1.1	Voltaite	Mina Alcaparrosa, Cerritos Bayos, Calama, Chile	DD104
29.9.1.3	Pertlikite	Madeni, Iran	Mg-voltaite
30.2.5.1	Jarosite	Sierra Pena Blanca Aldina, Chihuahua, Mexico	132060
30.2.5.1	Jarosite	Sierra Gorda, Chile	SPT113
30.2.5.1	Jarosite	Arabia District, Pershing Co., NV	SPT115
30.2.5.1	Jarosite	Copiapa Jarosite Mine, Dona Ana Co., NM	SPT116
30.2.5.1	Jarosite	Rustler Mine, Tooele Co., UT	SPT120
30.2.5.6	Plumbojarosite	Lomo de Toro Mine, Zimapan, Hidalgo, Mexico	ML-S15
31.8.3.1	Sideronatrite	Chuquicamata, Chile	115164
31.8.3.2	Sideronatrite	Crescent Valley, CA	SPT123[3]
31.8.4.1	Metasideronatrite	Chuqulcamata, Antofagasta, Chile	VZO112[4]
31.8.4.1	Metasideronatrite	Chuqulcamata, Antofagasta, Chile	105774-2[5]
31.9.1.1	Butlerite	Locality unknown; Mount Holyoke College collection	639[2]
31.9.1.1	Butlerite	Mina Quetena, Calama, Chile	C5534
31.9.1.1	Butlerite	Borate, Calico Hills, San Bernardino, CA	R7653
31.9.1.1	Butlerite	Riotorto, Tuscany, Italy-Ralph Dietz Collection	ML-S88
31.9.2.1	Parabutlerite	Chuquicamata, Antofagasta, Chile	157716[2]
31.9.2.1	Parabutlerite	Saghand Yazd, Iran	VZO115/116[2]
31.9.5.1	Metahohmannite	Quetena, Antofagasta, Chile	R12495[6]
31.9.6.1	Botryogen	Mina Santa Elena, La Alcaparrosa, Argentina	DD112[2]
31.9.6.1	Botryogen	unknown	G3775[2]
31.9.6.1	Botryogen	Redington Mine, Knoxville, Napa Co., CA	SPT124
31.9.6.2	Zincobotryogen	Mina Quetana, Calama, Chile	C5525-3
31.9.12.1	Slavikite	Valachov, Czech Republic	140229
31.9.12.1	Fibroferrite	Skouriatissa, Cyprus	SPT121
31.9.12.1	Fibroferrite	Borate, Calico Hills, San Bernardino, CA	VZO107/108[3]
31.9.12.1	Slavikite/gypsum	unknown	VZO122/123
31.10.5.1	Copiapite	Alma Pyrite Mine, Oakland, Alameda Co., CA	ML-S86
31.10.5.1	Copiapite	Alma Pyrite Mine, Oakland, Alameda Co., CA	SPT117
31.10.5.4	Ferricopiapite	Sulfur Mine, Contrary Creek, Mineral, Louisa Co., VA	168257[7]
31.10.5.4	Ferricopiapite	Sierra Gorda, Chile	ML-S35
31.10.5.4	Ferricopiapite	Borate, San Bernardino Co., CA	SPT 109[8]
31.10.5.4	Ferricopiapite	Sierra Gorda, Chile	SPT125
31.10.5.4	Ferricopiapite	Alcaparrosa, Chile	SPT133
30.10.5.6	Zincocopiapite	unknown	G-3637[8]

Notes: [1] XRD not available on this sample, so NMNH identification was used. [2] XRD not available on this sample. [3] Sample has small unidentified impurity. [4] XRD identified this sample as serpierite + metasideonatrite. [5] XRD found this sample to be 50% metasideronatrite and ~50% kanemite; the latter is nominally Fe-free. Metasideronatrite is not in the XRD database. [6] XRD of very small sample showed mixture of unspecified phases. [7] XRD not available on this sample. [8] XRD suggests presence of minor metavoltine impurity.

However, as noted at the onset, quadrupole splitting (Δ) varies considerably among the various sulfates studied here. It is thus convenient to group and discuss the Fe^{3+} doublets in sulfates according to quadrupole splitting.

Lowest Δ sulfates

Some of the most unusual Mössbauer spectra found in the sulfates belong to members of the hydration series $Fe_2(SO_4)_3 \cdot nH_2O$, which includes quenstedtite, coquimbite, kornelite, and lausenite (Table 3). All these minerals have Mössbauer spectra (Fig. 3) that closely resemble singlets because of their low quadrupole splitting, which in turn implies that there is only a negligible electric field gradient at the nucleus of the Fe^{3+} cation.

In quenstedtite, $Fe_2^{3+}(SO_4)_3 \cdot 11H_2O$, there are two types of clusters: *cis*-$[Fe^{3+}(SO_4)_2(H_2O)_4]$ and $[Fe^{3+}(SO_4)(H_2O)_5]$, along with H_2O groups (Thomas et al. 1974; Hawthorne et al. 2000). However, the coordination polyhedra occupied by Fe^{3+} cations in these clusters are still very similar despite the difference between five vs. four O^{2-} anions (Fig. 3). Thus the Mössbauer spectrum of quenstedtite consists of two highly overlapping doublets with very small Δ values, one of which is nearly a singlet. Its parameters are δ = 0.47 and 0.40 mm/s and Δ = 0.13 and 0.24 mm/s.

Perhaps the most commonly occurring (on Earth) sulfate species in this group is coquimbite $[Fe_2^{3+}(SO_4)_3 \cdot 9H_2O]$. The major feature in four of the samples studied here is again nearly a singlet, with parameters of roughly δ = 0.46 mm/s and Δ = 0.09 mm/s. Its structure, along with its polytype paracoquimbite (Fang and Robinson 1970), is composed of isolated clusters of $[Fe_3^{3+}(SO_4)_6]$ along with $[Fe^{3+}(H_2O)_6]$ octahedra and (H_2O) groups. The Fe octahedra are slightly different in geometry. As seen in

TABLE 3. Mössbauer parameters of low Δ sulfates containing dominantly Fe^{3+}

Mineral	Fig.	Sample	δ	Δ	area	δ	Δ	area	δ	Δ	area	δ	Δ	area	δ	Δ	area	δ	Δ	area	δ	Δ	area
Quenstedtite	3	B8255				0.47	0.13	35	0.40	0.24	65												
Coquimbite		VZO101/102	0.18	0.58	7	0.46	0.10	93															
		SPT132	0.18	0.71	6				0.42	0.47	94												
		SPT131	0.19	0.72	9				0.43	0.44	91												
	3	SPT126/127	0.16	0.66	5	0.45	0.08	95															
		SPT119	0.16	0.77	5	0.47	0.09	95															
		ML-S63				0.44	0.25	86	0.35	1.09	7	0.31	0.58	7									
		R7661	0.19	0.52	7	0.46	0.11	93															
Kornelite	3	R16185				0.44	0.11	100															
Lausenite	3	102923				0.47	0.12	89										1.25	2.63	6			
Ferrinatrite		VZO105/106[1]							0.44	0.40	88	0.40	1.13	12									
	3	R6214[2]				0.47	0.05	100															
Voltaite		DD104	0.13	0.47	13				0.46	0.40	36				1.35	1.82	43	1.42	2.28	8			
		137958							0.46	0.37	34				1.22	1.60	17	1.33	1.77	29	1.26	2.83	21
		158795	0.14	0.61	7				0.47	0.37	45				1.20	1.58	24	1.34	1.62	23			
	3	129313	0.10	0.54	7				0.43	0.35	35				1.26	1.79	58						
		115035	0.11	0.59	10				0.47	0.38	48				1.34	1.62	26	1.20	1.63	16			
		85679	0.16	0.69	9				0.43	0.36	40				1.30	1.79	32	1.19	1.75	19			
		95830†				0.34	0.37	12	0.54	0.38	43				1.15	1.69	23	1.31	1.63	15	1.09	2.46	7
Pertlikite	†	pertlikite							0.42	0.36	72				1.30	1.70	13	1.18	1.65	12			
Rhomboclase		ML-S84				0.54	0.43	23	0.43	0.53	77												
		ML-S85							0.44	0.52	97												
	3	ML-S89							0.44	0.51	97												
		81268							0.44	0.54	95												

Notes: Values for δ and Δ are given in mm/s and areas are given as percentage of the total spectra area. Errors bars are ±0.02 mm/s for δ and Δ and ±1–5% on doublet areas. Doublets with peak areas <5% of the total area are not included in this table. Their parameters, peak widths and goodness of fit parameters for all spectra are given in Table 2, in supplementary materials. † Spectrum of this sample was published in Ertl et al. (2012).
[1] Sample also contains minor metavoltine. [2] Sample also contains a coquimbite impurity.

TABLE 4. Mössbauer parameters of predominantly Fe^{3+} sulfate minerals with Δ of 0.31–0.81 mm/s*

Mineral	Fig.	Sample	δ	Δ	area	δ	Δ	area	δ	Δ	area	δ	Δ	area	δ	Δ	area	δ	Δ	area	δ	Δ	area
Yavapaiite	4a	ML-579				0.48	0.31	100															
Krausite	4a	156916				0.41	0.41	100															
Goldichite	4a	123922	0.19	0.61	29	0.48	0.29	71															
Copiapite	4a	SPT117	0.21	0.34	6	0.42	0.35	43				0.43	0.79	41	0.34	1.00	10						
		G596-1													0.37	1.18	100						
Ferricopiapite		SPT125				0.42	0.40	38				0.43	0.77	38	0.38	1.18	25						
		ML-S35				0.43	0.39	35	0.37	0.52	16	0.43	0.78	48									
		168257				0.42	0.37	26				0.43	0.78	17				1.25	2.71	51			
	4a	SPT 109				0.42	0.36	38				0.42	0.74	62									
		SPT133				0.42	0.40	40	0.38	0.53	27	0.43	0.76	33									
Zincocopiapite	4a	G-3637	0.07	0.45	7	0.43	0.38	42				0.43	0.88	50									
Apjohnite	4b	121356	0.19	0.75	12	0.43	0.58	70													1.27	3.31	18
Bilinite	4b	169017	0.09	0.79	17	0.49	0.37	71										1.37	1.78	7	1.06	3.69	5
Dietrichite	4b	G-2429				0.42	0.35	44	0.43	0.79	52												
Römerite		SPT110				0.43	0.55	23	0.29	0.61	30							1.23	2.87	12	1.28	3.01	35
		SPT122/126													1.39	2.09	23†	1.27	2.74	44	1.27	3.27	7
	6b	113733	0.17	0.61	6	0.44	0.37	69	0.39	0.39	2										1.27	3.28	23
		159098-2	0.15	0.64	7	0.46	0.36	49										1.26	2.73	27	1.26	3.30	18
		C5602-1	0.15	0.58	7	0.45	0.33	50										1.28	2.76	32	1.27	3.30	11
		93825	0.16	0.60	5	0.44	0.33	55										1.29	2.78	25	1.29	3.31	15
		R8415	0.17	0.56	12	0.47	0.36	56	0.36	0.37	7							1.34	2.59	2	1.29	3.29	23
Metavoltine		VZO114				0.43	0.35	53							0.40	1.04	36						
															1.16	2.01	11						
		G2677				0.44	0.24	19													1.27	3.23	81
	4b	SPT109				0.33	0.46	19	0.42	0.37	38	0.43	0.74	43									
Starkeyite	4b	ML-S65	0.16	0.64	61																		
			0.06	0.49	39																		
Ilesite	3b	123277							0.31	0.62	97												

Notes: Values for δ and Δ are given in mm/s and areas are given as percentage of the total spectra area. Errors bars are ±0.02 mm/s for δ and Δ and ±1–5% on doublet areas.
* Doublets with peak areas <5% of the total area are not included in this table. Their parameters, peak widths, and goodness of fit parameters for all spectra are given in Table 2, in supplementary materials. † Likely an impurity.

Figure 3, the A11 and Fe2 sites are nearly identical, although the Fe1 site is distinct. This implies that there may be two different Fe^{3+} doublets in coquimbite, and this is indeed observed. The doublet with very low Δ just noted is most likely assigned to the $[Fe^{3+}_3(SO_4)_6]$ site because that site is most similar to that in quenstedtite. The other group of samples containing coquimbite (SPT131, SPT132, and S63) has spectra dominated by a doublet with larger Δ and will be discussed later. Note that the sample of paracoquimbite studied here is mostly Fe^{2+} but its Fe^{3+} doublet matches one of the doublets in coquimbite ML-S63.

When these clusters depolymerize, they form the same chains found in two closely related hydration states of kornelite and lausenite. Kornelite $[Fe^{3+}_2(SO_4)_3{\cdot}7H_2O]$ is composed of spiral chains of $[Fe^{3+}(H_2O)_6]$ octahedra and SO_4 tetrahedra, cross-linked by additional SO_4 tetrahedra. The structure also includes partially occupied sites between the chains, making

TABLE 5. Mössbauer parameters of Fe^{3+} sulfate minerals with predominantly high quadrupole splitting*

Mineral	Fig.	Sample	δ	Δ	area	δ	Δ	area	δ	Δ	area	δ	Δ	area	δ	Δ	area	δ	Δ	area
Butlerite	5a	C5534										0.41	0.96	100						
		R7653										0.41	0.95	100						
		639										0.41	0.98	100						
		ML-S88							0.41	0.80	81	0.42	0.99	19						
Parabutlerite	5a	VZO115/116										0.41	0.98	100						
		157716				0.42	0.40	38	0.42	0.75	50	0.37	1.20	12						
Slavikite	5a	140229	0.27	0.63	34	0.55	0.52	39				0.38	1.23	39						
		VZO122/123[1]				0.37	0.57	76				0.38	1.15	24						
Fibroferrite		SPT121				0.41	0.52	37	0.42	0.96	63									
	5a	VZO107/108				0.41	0.50	100												
Botryogen		SPT124													0.42	1.18	49	0.40	1.63	43
		G3775				0.41	0.35	30	0.41	0.80	31				0.37	1.25	34			
	5a	DD112													0.41	1.16	63	0.40	1.60	33
Zincobotryogen	5a	C5525-3													0.41	1.21	57	0.39	1.65	43
Sideronatrite	5b	SPT123													0.42	1.15	100			
		115164													0.41	1.15	100			
Metasideronatrite	5b	105774-2										0.35	1.20	43	0.44	1.18	57			
		VZO112										0.42	1.17	48	0.38	1.18	52			
Metahohmannite	5b	R12495										0.43	0.94	100						
Amarantite	5b	G3775				0.43	0.35	8				0.44	0.98	8	0.40	1.19	54	0.39	1.60	30
Jarosite	5b	132060													0.38	1.30	100			
		SPT113													0.38	1.18	100			
		SPT116													0.38	1.23	100			
		SPT115													0.38	1.29	100			
		SPT120										0.37	0.70	56	0.38	1.14	44			
Plumbojarosite†	5b	ML-S15	0.29	0.70	12							0.37	1.22	79				0.76	1.22	9
Anhydrite		159266‡				0.44	0.41	76	0.14	0.58	24									
	5c	SPT132‡				0.40	0.46	93				0.38	1.02	7						
Celestine	5c‡	ML-S13‡				0.15	0.54	65				0.24	0.87	35						

Notes: Values for δ and Δ are given in mm/s and areas are given as percentage of the total spectra area. Errors bars are ±0.02 mm/s for δ and Δ and ±1–5% on doublet areas.

* Doublets with peak areas <5% of the total area are not included in this table. Their parameters, peak widths and goodness of fit parameters for all spectra are given in Table 2, in supplementary materials.

† This sample also contains a magnetic sextet from an unknown impurity.

‡ Mössbauer data cannot determine whether the Fe in these samples is actually part of the sulfate's structure, or if it is an impurity. SPT132 is known from XRD to be a mixture of anhydrite and coquimbite, but XRD of 159266 and ML-S13 show that they are "pure." However, it takes only a tiny amount of Fe-rich sulfate impurity to have a large influence on the spectrum of a low-Fe Ca sulfate.

[1] XRD suggests this sample is gypsum but there is apparently some slavikite impurity here, given the similarity of this spectrum to the known slavikite 140229.

TABLE 6. Mössbauer parameters of predominantly Fe^{2+} sulfate minerals*

Mineral	Fig.	Sample	δ	Δ	area	δ	Δ	area	δ	Δ	area	δ	Δ	area	δ	Δ	area	δ	Δ	area	δ	Δ	area
Szomolnokite		ML-S77																1.26	2.73	94			
		92942																1.26	2.73	96			
		136685-2				0.54	0.14	7	0.23	0.69	12							1.29	2.74	82			
	6a	104276																1.28	2.76	100			
	6a	ML-S60																1.31	2.89	57	1.31	3.42	31
		159098				0.49	0.18	12							1.31	2.69	42	1.24	2.78	43			
		159266				0.46	0.36	72	0.14	0.56	28												
		ML-S103				0.43	0.42	7										1.27	2.74	93			
Szmikite	6a	159189							0.52	0.93	18							1.24	2.59	82			
Gunningite	6a	156925				0.26	0.40	32				0.37	1.26	10				1.25	2.74	58			
Chalcanthite	6a	DD100	0.10	0.51	29				0.26	0.76	30							1.26	2.32	22	1.30	2.88	19
Pentahydrite†	6a	VZO121							0.50	0.83	8							1.26	3.00	53	1.27	3.68	38
Jokokuite	6b	G3536	0.15	0.56	26										1.13	2.63	6	1.26	2.51	65			
Halotrichite	6b	G1616																			1.27	3.29	92
		VZO128	0.13	0.49	10	0.36	0.31	14							1.45	1.56	13	1.28	2.76	43	1.30	3.29	20
Melanterite	6b	2070																			1.27	3.21	100
Rozenite		JB626B																1.33	2.97	59	1.33	3.39	34
	6b	SPT130										0.39	0.95	8							1.27	3.21	92
Starkeyite	6b	137725	0.00	0.57	9													1.14	2.65	91			

Notes: Values for δ and Δ are given in mm/s and areas are given as percentage of the total spectra area. Errors bars are ±0.02 mm/s for δ and Δ and ±1–5% on doublet areas.

* Doublets with peak areas <5% of the total area are not included in this table. Their parameters, peak widths, and goodness of fit parameters for all spectra are given in Table 2, in supplementary materials.

† Sample known to include minor impurities from pickeringite, starkeyite, botryogen, and boussingaultite.

kornelite a heptahydrate. Early workers believed that lausenite $[Fe_2^{3+}(SO_4)_3 \cdot 5H_2O]$ had the kornelite structure with none of these extra water molecules (Robinson and Fang 1973), but more recent work by Majzlan et al. (2005) shows that a different arrangement is likely. In lausenite, the chains are tilted to free up one of the H_2O molecules, with bridging O atoms coordinating S^{6+} and Fe^{3+} (Majzlan et al. 2005). Two symmetrically distinct Fe^{3+} sites exist as seen in Figure 3; Fe^{3+} is coordinated either by four O and two H_2O (the Fe1 site) or three O and three H_2O (the Fe2 site). The Mössbauer spectra of kornelite and lausenite are quite similar. In three of the four samples, a doublet with $\delta = 0.48$ mm/s and $\Delta = 0.13$ mm/s dominates, quite like those found

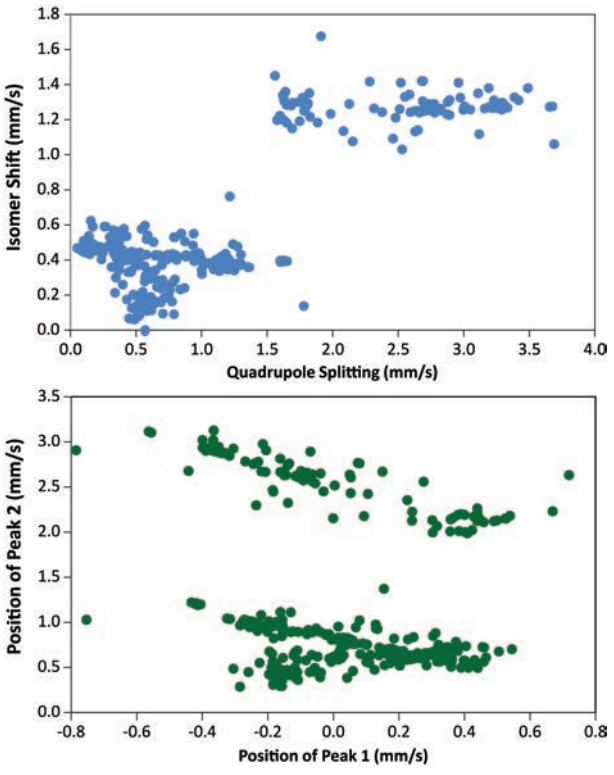

FIGURE 2. Mössbauer parameters of sulfates measured in this study. The top panel shows peak positions plotted in terms of isomer shift and quadruple splitting. The bottom panel shows the actual positions of the peaks, which follow a continuum across velocity space. (Color online.)

in coquimbite. The fourth sample, 104175, is mostly Fe^{2+} with a Fe^{3+} doublet with higher δ and Δ, probably due to an impurity. By way of comparison, Huggins and Huffman (1979) reported δ = 0.44 mm/s and Δ = 0.15 mm/s for kornelite.

Another related structure is that of ungemachite, $K_3Na_8[Fe^{3+}(SO_4)_6](NO_3)_2(H_2O)_6$, which is also based on clusters. Ungemachite belongs to the glaserite crystal structure type, in which an octahedron shares six corners with (SO_4) tetrahedra, forming pinwheels (Moore 1973). The pinwheels are then linked into tetrahedra to form layers. Many sulfate, phosphate, chromate, and silicate minerals are based on this structure, including millosevichite $[Al_2(SO_4)_3]$, glaserite $[K_3Na(SO_4)_2]$, and mikasaite $[Fe_2(SO_4)_3]$. An early paper by DeBenedetti et al. (1961) gave parameters for mikasaite of δ = 0.46 mm/s and Δ = 0.00 mm/s, while Nomura et al. (2005) reported values of δ = 0.47 mm/s and Δ = 0.34 mm/s. Sgarlata (1985) reported only a singlet at 0.44 mm/s for millosevichite $[Al_2(SO_4)_3]$. These data suggest that the glaserite structure-type minerals will all also have low-Δ values. Clearly, more work on a broader range of species would be useful to confirm this trend in the Mössbauer parameters of this structure type, which is largely unexplored.

Ferrinatrite, $Na_3(H_2O)_3[Fe^{3+}(SO_4)_3]$, is formally classified as a chain sulfate, but the linkages between $[Fe^{3+}(SO_4)_3]$ octahedral-tetrahedral chains create octahedra that are very similar to the clusters in coquimbite (Hawthorne et al. 2000), as can be seen in Figure 3. Mössbauer parameters of ferrinatrite (Table 3) are also indistinguishable from those of the $Fe(SO_4)_3{\cdot}nH_2O$ hydration series.

Voltaite $\{K_2[Fe^{2+}_5Fe^{3+}_3(H_2O)_{12}(SO_4)_{12}][Al(H_2O)_6]\}$ and the related Mg-rich species pertlikite (Ertl et al. 2008) have multiple Mössbauer doublets because there are two distinct octahedral sites occupied by Fe^{3+} and Fe^{2+}: 32 M1 and 96 M2 sites per unit cell. Ideally, Fe^{3+} occupies all of the M1 sites and the M2 sites are shared by both valence states of Fe. However, this mineral shows a great deal of variation among the eight samples studied here. Voltaite has one group of large doublets at δ = 0.44–0.54 mm/s and Δ = 0.35–0.40 mm/s, as well as a second group of smaller doublets at δ = 0.10–0.16 mm/s and Δ = 0.47–0.69 mm/s. All the samples studied here contained roughly equal distributions of Fe^{2+} and Fe^{3+}. Their spectra are similar in appearance to those of Long et al. (1980), but they did not publish δ and Δ for their Fe^{3+} doublets. Hermon et al. (1976) also had trouble resolving contributions from different Fe^{3+} doublets, but concluded that multiple doublets must be present on the basis of increasing linewidth at low temperatures. They suggested that the larger Δ Fe^{3+} doublet corresponds to the M2 site, while the less distorted M1 doublet had a smaller Δ. They also suggest that there may be some divalent cations in the smaller M1 site, even when there are trivalent cations in the larger M2 site. Majzlan et al. (2011) measured three samples, and obtained consistent parameters for two doublets with δ = 0.59 and 1.42 mm/s and Δ = 0.26 and 2.52–2.68 mm/s, respectively. These do not agree well with current results, but the reason for the discrepancy may lie in the fact that they only modeled two doublets. Majzlan et al. (2013) studied a large suite of synthetic voltaites and found parameters of δ = 0.45–0.47 mm/s and Δ = 1.29–1.31 mm/s that are closer to those from the current study and previous workers. Support for the fits used in the current study lies in the fact that doublets with the same parameters are also found in rhomboclase, where they are clearly resolved at >75% of the total spectral area.

Rhomboclase, $(H_5O_2)[Fe^{3+}(H_2O)_2(SO_4)_2]$, has a structure somewhat related to kornelite, in that it is also a sheet of SO_4 tetrahedra and $Fe^{3+}O_6$ octahedra. Two-dimensional linkages between adjacent clusters link them into sheets, with hydrogen bonding of interstitial $(H_5O_2)^+$ dimers (Hawthorne et al. 2000). Mössbauer parameters of δ = 0.54 and Δ = 0.59 mm/s were reported by Majzlan et al. (2011) and all five samples in the current study had those quite similar parameters: ca. δ = 0.44 mm/s and Δ = 0.51–0.54 mm/s. The Fe site in rhomboclase is apparently quite similar to the Fe1 site in voltaite, as is apparent in Figure 3.

Minerals with Δ = 0.31–0.81 mm/s

The Mössbauer spectrum of yavapaiite, $K[Fe^{3+}(SO_4)_2]$, is a single doublet with δ = 0.48 mm/s and Δ = 0.31 mm/s (Table 4; Fig. 4a). Those parameters match those reported for three samples by Nomura et al. (2005) almost exactly. Its structure is based upon sheets of SO_4 tetrahedra and $Fe^{3+}O_6$ octahedra that are created by corner sharing of $[Fe^{3+}(SO_4)O_2]$ chains (Hawthorne et al. 2000). The same sheet geometry is also found in kröhnkite $[Na_2Cu^{2+}(H_2O)_2(SO_4)_2]$, merwinite $[Ca_3Mg(SiO_4)_2]$, and brianite $[Na_2CaMg(PO_4)_2]$, as well as members of the fairfieldite sub-group of hydrated phosphates, so Fe^{3+} substitution in those structures should result in yavapaiite-like Mössbauer parameters. Krausite, $K[Fe^{3+}(H_2O)_2SO_4)_2]$, has a related structure based on

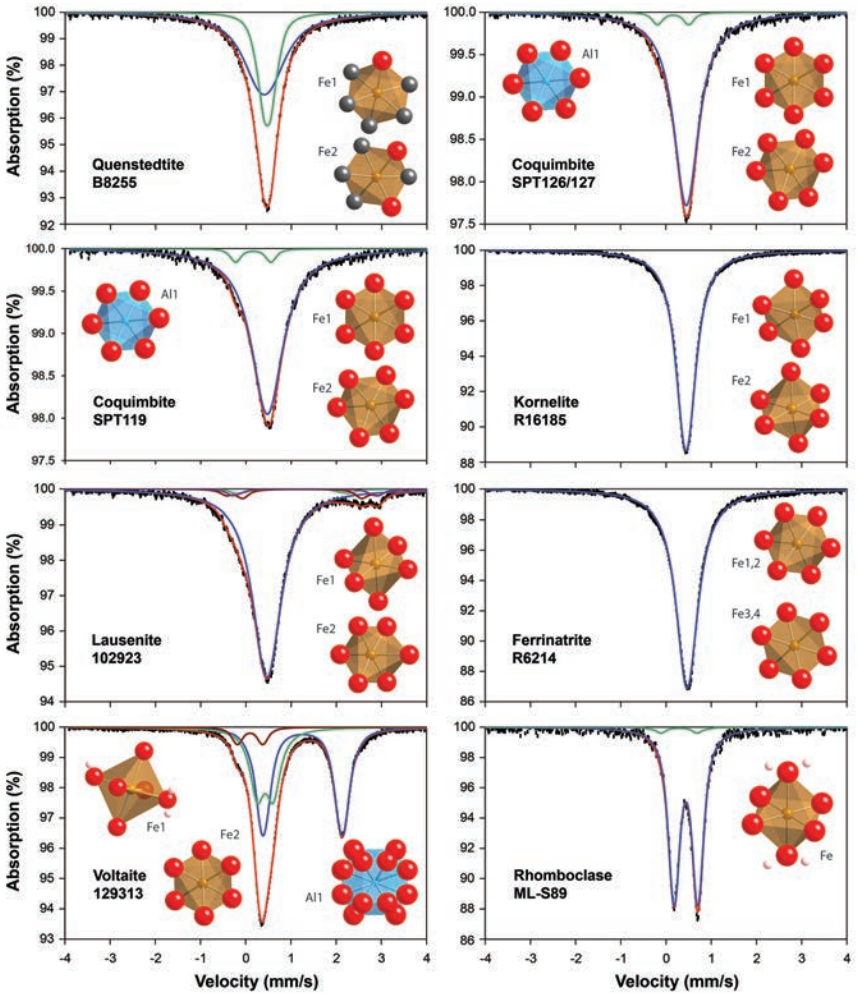

FIGURE 3. Mössbauer spectra and Fe coordination polyhedra in sulfates with very small Δ values less than ~0.35 mm/s. Data points are plotted are ±standard deviations but are cropped at the baseline, which is defined to be 100% absorption. Polyhedra were created using CrystalMaker software and data from the American Mineralogist Crystal Structure Database: quenstedtite (Thomas et al. 1974), coquimbite (Fang and Robinson 1970), kornelite (Robinson and Fang 1973), lausenite (Majzlan et al. 2005), ferrinatrite (Scordari 1977), voltaite (Mereiter 1972), and rhomboclase (Mereiter 1974). O atoms are shown in red, OH in gray, Al in blue, and Fe in orange. Note that XRD suggests that the R6214 ferrinatrite contains minor amounts of coquimbite that cannot be distinguished because the spectra are so similar. (Color online.)

infinite double chains like those found in kröhnkite (Graeber et al. 1965); its Mössbauer parameters of δ = 0.41 mm/s and Δ = 0.41 mm/s are similar to (though slightly higher than) those of yavapaiite. The Fe octahedra from the crystal structure refinements of these two minerals, as shown in Figure 4a, are slightly different. Note that the Fe site in krausite is slightly more distorted than the Fe site in yavapaiite, which would cause the higher Δ.

Goldichite [$KFe^{3+}(SO_4)_2{\cdot}4H_2O$] is a slightly higher hydration state of potassium ferric sulfate, such that the Fe^{3+} coordination polyhedron now has two *trans*-OH. Thus its Mössbauer spectrum is not the same as those of yavapaiite and the other structures based on infinite double chains. Rather, goldichite has two Fe^{3+} doublets with parameters, one with δ = 0.19 mm/s and Δ = 0.61 mm/s as seen in coquimbite, and one with δ = 0.48 mm/s and Δ = 0.29 mm/s comparable to yavapaiite and krausite. The structure of kainite {$K_4[Mg_4(H_2O)_{10}(SO_4)_4](H_2O)Cl_4$} is also based on kröhnkite-like chains, and probably has Mössbauer parameters like krausite. All these minerals have quite similar Mössbauer spectra (Fig. 4a).

Copiapite group minerals share the general formula $[Fe^{3+}_2(OH)(H_2O)_4(SO_4)_3]_2[A(H_2O_6)](H_2O)_6$, where $A = Fe^{2+}$, Fe^{3+}, Al, Mg, Cu, Ca, and/or Zn (Hawthorne et al. 2000). Their structures are composed of layers of the $[A(H_2O_6)]$ octahedra that are linked to layers of $[Fe^{3+}_2(OH)(H_2O)_4(SO_4)_3]$, forming $[M_2(SO_4)_2(O,H_2O)_7]$ clusters that resemble those in phosphates (Hawthorne 1979). Only one sample studied here (168257) had an Fe^{2+} doublet with 51% of the total area, defining it to be copiapite rather than ferricopiapite. All the other copiapite samples in the data set studied here have only Fe^{3+}, and so are really ferricopiapite despite the species names given to them, and the single zincocopiapite sample has identical Mössbauer parameters to those of the ferricopiapites. The ferricopiapites have two distinct distributions

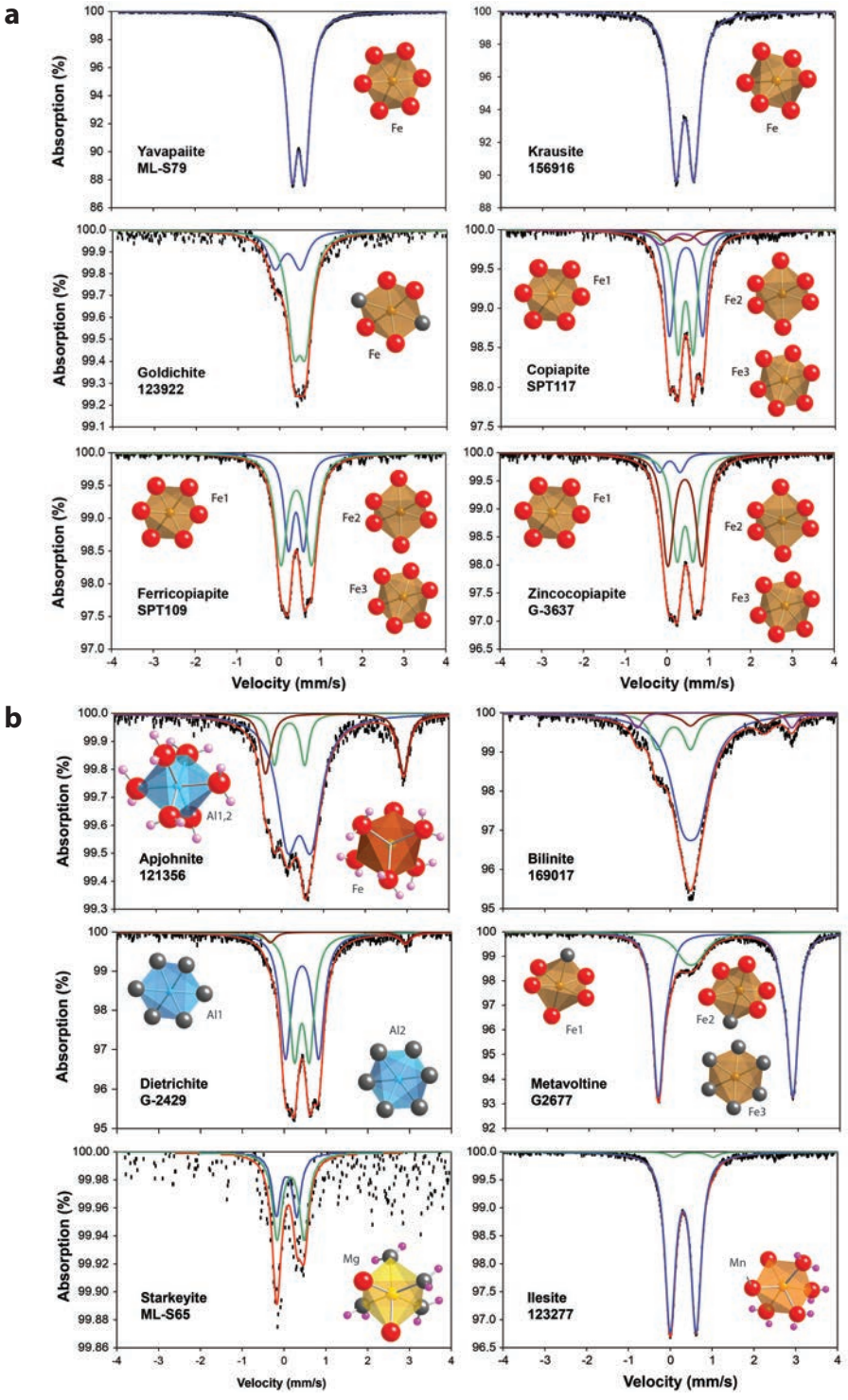

FIGURE 4. (**a**) Mössbauer spectra and Fe coordination polyhedra in sulfates with Δ values between ~0.31 and 0.74 mm/s. Polyhedra were created using CrystalMaker software and data from the American Mineralogist Crystal Structure Database: yavapaiite (Graeber and Rosenzweig 1971), krausite (Graeber et al. 1965), goldichite (Graeber and Rosenzweig 1971), copiapite, ferricopiapite, and zincocopiapite (Fanfani et al. 1973). O atoms are shown in red, OH in gray, and Fe in orange. (**b**) Mössbauer spectra and Fe coordination polyhedra in sulfates with Δ values between 0.58 and 0.79 mm/s. Polyhedra were created using CrystalMaker software and data from the American Mineralogist Crystal Structure Database: apjohnite (Menchetti and Sabelli 1976), dietrichite (Ballirano et al. 2003), metavoltine (Giacovazzo et al. 1976), starkeyite (Baur 1962), and ilesite (Held and Bohaty 2002). No crystal structure is available for bilinite. O atoms are shown in red, OH in gray, H in pink, Mg in yellow, Al in blue, and Fe in orange. Metavoltine G2677 has a römerite impurity (large QS doublet); its Fe^{3+} feature is nearly a singlet, as also seen in bilinite. (Color online.)

of Mössbauer parameters with the same δ = 0.42–0.43 mm/s but different quadrupole splittings: Δ = 0.35–0.40 mm/s for one group and 0.77–0.88 mm/s for the other. These probably correspond to sites in the two different layers mentioned above but it is unclear at this point, which doublet represents which site. Two similar sites were observed in Mössbauer spectra of samples from the Río Tinto basin in Spain by Fernández-Remolar et al. (2005): δ = 0.37 and 0.39 mm/s and Δ = 0.34 mm/s and 0.74 mm/s, respectively. Majzlan et al. (2011) also reported copiapite data with parameters of δ = 0.53 mm/s and Δ = 0.30–0.38 and 0.79–0.80 mm/s.

Halotrichite group minerals share a structure with $[M(SO_4)_2(H_2O)_4]$ clusters of M^{2+} and M^{3+} octahedral cations. The two $[M^{3+}(H_2O)_6]$ octahedra are charge balanced by the presence of $[M^{2+}(SO_4)(H_2O)_5]$ octahedra, with an additional five H_2O molecules held in place by hydrogen bonding (Hawthorne 1985). Three Fe^{3+}-rich halotrichite group minerals were studied here, apjohnite, bilinite, and dietrichite, and their Mössbauer spectra (Fig. 4b) are somewhat similar. The main feature in the apjohnite spectrum is a large doublet with δ = 0.43 mm/s and Δ = 0.58 mm/s, similar to that of rhomboclase. The bilinite spectrum has a broad doublet at δ = 0.49 mm/s and Δ = 0.37 mm/s, identical to one of the doublets in copiapite. Dietrichite has two doublets with δ = 0.42 and 0.43 mm/s and Δ = 0.35 and 0.79 mm/s.

In the very-similar römerite structure, Fe occupies octahedral sites that are parts of an analogous $Fe(SO_4)_2(H_2O)_4$ cluster (Fig. 1). As in the halotrichite group, the clusters have a *cis* arrangement of polyhedra (Fig. 4b). In addition to the cluster, Fe in römerite is also found in isolated $[Fe^{2+}(H_2O)_6]$ octahedra. Several different examples of römerite were obtained, and nearly all the samples contain both Fe^{2+} and Fe^{3+}. These minerals should have Fe^{3+} parameters similar to those for the halotrichite minerals, and this is indeed what is observed: δ_{Bil} = 0.49 mm/s and Δ_{Bil} = 0.37 mm/s, while $\delta_{Röm}$ = 0.43–0.47 mm/s and $\Delta_{Röm}$ = 0.23–0.55 mm/s. Huggins and Huffman (1979) found similar parameters for two doublets in römerite of δ = 0.38 and 0.53 mm/s and Δ = 0.37 and 0.25 mm/s, respectively, while Majzlan et al. (2011) reported δ = 0.52 and 0.59 mm/s, with Δ = 0.38 and 0.17 mm/s (note again that their δ values are slightly high). They also observed the Fe^{2+} doublet with δ = 1.38 and Δ = 3.49 mm/s.

Metavoltine $\{K_2Na_6[Fe^{3+}_3O(SO_4)_6(H_2O)_3]_2[Fe^{2+}(H_2O)_6](H_2O)_6\}$ is related to römerite because it is also based on isolated clusters, in this case with composition $[Fe^{3+}_3(SO_4)_6O(H_2O)_3]$, and the clusters are linked by hydrogen bonding (Hawthorne 1985). There are three Fe sites: two for Fe^{3+} that occur within the clusters [Fe(1) and Fe(2)], and those in isolated Fe(3) octahedra that the formula suggests should be strictly Fe^{2+} (Giacovazzo et al. 1976). As would be appropriate for the formula given above, the spectra have predominantly Fe^{3+} features. One doublet has δ = 0.33–0.44 mm/s and Δ = 0.24–0.46 mm/s, a second has parameters of δ = 0.38–0.42 mm/s and Δ = 0.37–0.53 mm/s, and a third has δ = 0.43 mm/s and Δ = 0.74–0.76 mm/s. All have comparable areas, suggesting that some Fe^{3+} is occupying the Fe sites in the structure equally. Sgarlata (1985) reported parameters of δ = 0.43 mm/s and Δ = 0.36 mm/s for Fe^{3+} in metavoltine, similar to those observed for the first doublet.

As noted above, there are two different types of sites in coquimbite: isolated clusters of $[Fe^{3+}_3(SO_4)_3]$ and $[Fe^{3+}(H_2O)_6]$ octahedra. In some samples, only a doublet with very small quadrupole splitting (~0.10 mm/s) is observed, and stoichiometry suggests that this must represent Fe^{3+} in both sites. However, several of the samples studied here instead have a doublet with higher Δ that is very similar to the Fe^{3+} doublet in römerite (which also has two distinct octahedral sites), with parameters of δ = 0.42 mm/s and Δ = 0.44–0.47 mm/s. This higher Δ doublet is found in multiple samples from different parageneses that have been positively identified by XRD, so the existence of an impurity is unlikely. It was also reported by Pankhurst et al. (1986), who gave δ = 0.35–0.36 mm/s and Δ = 0.56–0.60 mm/s. It is likely that substitution of other cations (such as Mg and Al) may be lowering the symmetry of the site, thus increasing its quadrupole splitting. Both XRD and reflectance spectroscopy (Lane et al., in review) confirm that all the samples studied contain coquimbite, so the observed variations in site occupancy must be due to formation conditions or other unknown crystal chemical constraints.

Taken together with the very low-Δ doublets observed in all coquimbite samples studied here, the coquimbite data corroborate the work of Huggins and Huffman (1979), who found doublets with δ = 0.51 and 0.43 mm/s and Δ = 0.00 and 0.26 mm/s, respectively. Fernández-Remolar et al. (2005) could not easily distinguish a doublet assigned to coquimbite and reported slightly high parameters of δ = 0.44 mm/s and Δ = 0.22 mm/s. The higher values of Δ from these workers may represent unresolved contributions from a doublet with higher Δ, or they may represent variations in Mössbauer parameters as a function of some unrecognized compositional effect.

The isostructural rozenite group minerals (rozenite, $FeSO_4{\cdot}4H_2O$, starkeyite, ilesite, aplowite, and boyleite) are based on clusters, which might suggest that their Mössbauer parameters should be similar to those of halotrichite, metavoltine, and coquimbite. Each cluster is composed of two tetrahedra each sharing two corners with two octahedra; the resultant formula is $M_2(SO_4)_2O_8$, where M = Fe, Mg, Mn, Co, and/or Zn. In the sample suite studied here, minerals in this group are dominantly Fe^{2+}-rich and will thus be discussed below in section G; only a few tiny doublets (<2% of the total spectral area) with very scattered parameters are observed for Fe^{3+} in rozenite. However, the Mössbauer spectrum of a low-Fe starkeyite gave parameters like those of römerite, with δ = 0.16 and 0.06 mm/s and Δ = 0.64 and 0.49 mm/s. Ilesite (the Mn equivalent of rozenite) contains only Fe^{3+}, with parameters of δ = 0.31 mm/s and Δ = 0.62 mm/s.

Within this group of sulfates based on linked clusters (Figs. 3, 4a, and 4b), it should be apparent that no mineral species has a diagnostic or truly characteristic Mössbauer spectrum. Due to the similarities in their crystal structures and the resultant effect on the geometries of the Fe coordination polyhedra, none of these mineral species could be uniquely identified on the basis of their Mössbauer spectra alone.

Octahedral corner-sharing chain structures

A large group of sulfates with related structures is represented by a continuum of Mössbauer parameters with Δ ranging from ~0.80–1.2 mm/s. Their spectra are all quite similar, as seen in Figures 5a and 5b. This group includes butlerite and

parabutlerite, slavikite, fibroferrite, botryogen, sideronatrite, metasideronatrite, metahohmannite, and the alunite group. What do all these minerals have in common?

All but alunite have structures composed of infinite chains of SO_4 tetrahedra and $M(O,H_2O)_6$ octahedra, as noted by and described in Moore (1970). The chains have a repeat distance of ~7 Å (see butlerite in Fig. 1). In butlerite and parabutlerite, the tetrahedra alternate along the chain, linking to vertices of the octahedra (Hawthorne et al. 2000). The structure of slavikite is based on open sheets of corner-sharing octahedra and tetrahedra that are similar to fragments of the chains found in butlerite (Hawthorne et al. 2000); the Mössbauer spectra could thus be indistinguishable.

Sakai et al. (1981) reported the 300 K spectrum of butlerite to have δ = 0.42 mm/s and Δ = 0.94 mm/s, and parameters for three samples from this study are an excellent match: δ = 0.41 mm/s and Δ = 0.95–0.98 mm/s. One of the parabutlerite samples in this study is consistent, with δ = 0.41 mm/s and Δ = 0.98 mm/s, but sample 157716 is not. The latter has three distributions with parameters of δ = 0.22, 0.58, and 0.34 mm/s and Δ = 0.55, 0.54, and 1.14 mm/s. X-ray diffraction confirms that this sample is indeed parabutlerite, so these three doublets must represent a different cation ordering than is found in the other samples.

Moore (1970) notes the structural similarity of the chains in butlerite to those in the phosphate mineral laueite $[Mn^{2+}Fe_2^{3+}(OH)_2(H_2O)_6(PO_4)_2{\cdot}2H_2O]$ and its isotypes. Coincidentally, data on laueite from Monmouth County, New Jersey (Segeler et al. 2012) have a broad doublet corresponding to Fe^{3+} parameters of δ = 0.41 and Δ = 0.66 mm/s for the unresolved contributions of Fe in the M1 $[M^{2+}(H_2O)_4(PO_4)_2]$ and M3 $[Fe^{3+}(H_2O)_2(OH)_2(PO_4)_2]$ sites and δ = 0.40 and Δ = 1.29 mm/s for the M2 site $[Fe^{3+}(OH_2)(PO_4)_4]$. Several other phosphate minerals such as tancoite, paravauxite, wavellite, eosphorite, and strunzite share this same chain structure, and should also have the same Mössbauer parameters.

The slavikite structure (Parafiniuk et al. 2010) is composed of open sheets of corner-sharing octahedra and tetrahedra (Hawthorne et al. 2000), but the fragments are similar to those in the butlerite 7 Å chain (compare in Fig. 5a). Both Mössbauer spectra of slavikites have a doublet at δ = 0.36 mm/s and Δ = 1.14 mm/s like those in butlerite. Sample 140229 also contains Fe^{3+} in copiapite-like sites, with δ = 0.22 and 0.58 mm/s and Δ = 0.55 and 0.54 mm/s, while the second slavikite, VZO122/123, is dominated by a doublet with δ = 0.37 and Δ = 0.57 mm/s.

Similar chains are found in fibroferrite, although the linkages are with the *cis*-corners (compare parabutlerite and fibroferrite in Fig. 5a) rather than the *trans*-corners of the octahedra in butlerite. This difference must not affect the geometry of the Fe coordination polyhedra very much, because the fibroferrite samples in this study have parameters quite similar to those of slavikite and parabutlerite.

The structures of the botryogen group minerals and sideronatrite are also based on 7 Å chains (Hawthorne et al. 2000). It is thus no surprise that Fe^{3+} in these octahedra all give rise to similar Mössbauer parameters, although they are noticeably different than those from butlerite and related phases just discussed. All the botryogen, sideronatrite, and metasideronatrite spectra are dominated by the same doublet with δ = 0.41 mm/s and Δ = 1.14–1.21 mm/s. Botryogen is also related to and in the same Strunz classification group as copiapite; recall from discussion above that copiapite also has a doublet with parameters of δ = 0.42–0.43 mm/s and Δ = 0.77–0.80 mm/s. In addition to the doublets with $\Delta \approx$ 1.15 mm/s, other samples of botryogen also have a second doublet in their Mössbauer spectra with an unusually high Δ = 1.63 mm/s. This probably represents Fe^{3+} occupancy in the "branching" octahedra that link to the sides of the 7 Å chains. The botryogen and sideronatrite structures are again based on 7 Å chains, and the Fe coordination polyhedra are nearly identical (compare Figs. 5a and 5b).

Metahohmannite, hohmannite, and amarantite are all members of the amarantite group, and are intimately related by dehydration (hohmannite in particular is not stable under ambient conditions). Metahohmannite has Mössbauer parameters of δ = 0.43 mm/s and Δ = 0.94 mm/s exactly like those found in butlerite, parabutlerite, and fibroferrite. Amarantite, on the other hand, most closely matches botryogen (δ = 0.40 mm/s and Δ = 1.19 mm/s). The difference is that metahohmannite and amarantite include an OH^- group substituting for O^{2-} in the structure (Scordari et al. 2004), but both are still based on the aforementioned 7 Å chains.

Alunite group

The alunite group minerals, which include both alunite and jarosite, are composed of $[M^{3+}(OH)_6(SO_4)_2]$ sheets, where M is most commonly Fe^{3+} and/or Al^{3+}; monovalent and divalent cations such as K, Na, or H_3O^+ lie between the sheets. The Fe atoms occupy octahedra arranged in six-membered, corner-sharing rings as well as three-membered rings (Hawthorne et al. 2000). Mössbauer spectra of alunite group minerals have been studied extensively by numerous workers (Grinkevich and Kul'gavchik 1963; Hrynkiewicz et al. 1965; Herzenberg and Toms 1966; Takano et al. 1968; Afanasev et al. 1974; Johnston 1977; Leclerc 1980; Huggins et al. 1983; Taneja and Jones 1984; van der Kraan et al. 1984; Audley et al. 1986; Pax and Clark 1988; Gracia et al. 1990; Gancedo et al. 1992; Musíc et al. 1994; Morris et al. 1996; Herbert 1997; Ahmed et al. 1999, 2003, Fajardo et al. 1999; Ristić et al. 2005; Verma and Tripathi 2000; Waanders et al. 2003; Reyes et al. 2003; Ribeiro et al. 2003; Eneroth and Koch 2004; Rodríguez et al. 2005). Reported parameters range from δ = 0.30–0.45 mm/s and Δ = 1.00–1.22 mm/s, with most Δ values between 1.18 and 1.21 mm/s. The work of Rothstein (2006) and Dyar et al. (2006b) suggests that synthetic compositions across the compositional range of K-Na-H_3O^+ for jarosite have indistinguishable Mössbauer parameters, although there may be a relationship between isomer shift and Fe^{3+}/Al, with δ = 0.39 mm/s for Fe^{3+} end-members and δ = 0.37 mm/s for Al-rich ones. The jarosite spectra are nearly indistinguishable from sideronatrite and match those of botryogen and metasideronatrite very closely although the structures are not specifically related.

Other ferric-bearing sulfates

This study also included two samples of anhydrite and one of celestine. As Ca- and Ba-dominated sulfates, respectively, they do not fall in the same hierarchy as those previously discussed

here. The relatively large size of the Ca and Ba cations requires large sites in the structures, which are usually 8–12-coordinated. Anhydrite is based on chains of alternating edge-sharing SO_4 tetrahedra and CaO_6 dodecahedra (Hawthorne et al. 2000) linked by edge and corner sharing between chains (Fig. 1). Celestine consists of isolated SO_4 tetrahedra cross-linked by 12-coordinated Sr and Ba atoms (Brigatti et al. 1997). Thus these structures would seem unlikely to incorporate Fe^{3+} in their structures, although Fe^{2+} might substitute. However, their Mössbauer spectra are both dominated by Fe^{3+}. For sample SPT132, the identification of the impurity as coquimbite by XRD is consistent with the Mössbauer parameters of the largest doublet. XRD of the celestine ML-S13 and anhydrite 159132 showed no impurities, but given the crystal structural constraints, it is unlikely that this Fe^{3+} is not actually in the anhydrite or celestine; rather, it is reasonable to assume that it arises from an impurity of another Fe^{3+} phase. The anhydrite localities studied both include phosphates, so it is also possible that the impurity could be some Fe^{3+} phosphate. The phase assemblage of the Michigan locality of the celestine is unreported. However, celestine from the Moldanubian Zone of the Bohemian Massif in the Czech Republic has been reported with anhydrite, pyrite, pyrrhotite, and chalcopyrite, and parameters in this study are consistent with those possibilities.

Ferrous iron

It is again convenient to group and discuss the Fe^{2+} doublets in sulfates according to quadrupole splitting, which arises from a distribution of surrounding charges with less than cubic symmetry. Some samples in which Fe^{3+} features dominate merit revisiting because of their significant Fe^{2+} contents. The lowest values of Fe^{2+} quadrupole splitting in this study belong to voltaite (Table 3), with doublets at $\delta = 1.15–1.35$ mm/s and $\Delta = 1.58–1.82$ mm/s. Multiple doublets are found due to the presence of two M sites in the structure (both octahedral), as noted above in the section on Fe^{3+} in voltaite. The M1 site is coordinated to six O atoms from adjacent SO_4 tetrahedra, and has a slight trigonal distortion. It is the smaller of the two sites, with an average Fe-O distance of 2.004 Å (Mereiter 1972). This site may contain either Fe^{2+} or Fe^{3+}, according to the work of Long et al. (1980). The larger of the sites is designated the M2 site (with a multiplicity of three relative to one M1). It is coordinated to $FeO_4(H_2O)_2$, with Fe-O distances of 2.097 Å and Fe-H_2O distances of 2.075 Å (Mereiter 1972). Because of its size, only Fe^{2+} and larger cations occupy this site. Mössbauer results from this study agree very well with work by Long et al. (1980), who report values of $\delta_{M2} = 1.17–1.27$ mm/s and $\Delta_{M2} = 1.59–1.80$ mm/s. They also identified a second peak assigned to the $^{[M1]}Fe^{2+}$ site as well as a $^{[M2]}Fe^{3+}$ peak, but neither one was sufficiently resolved to determine parameters.

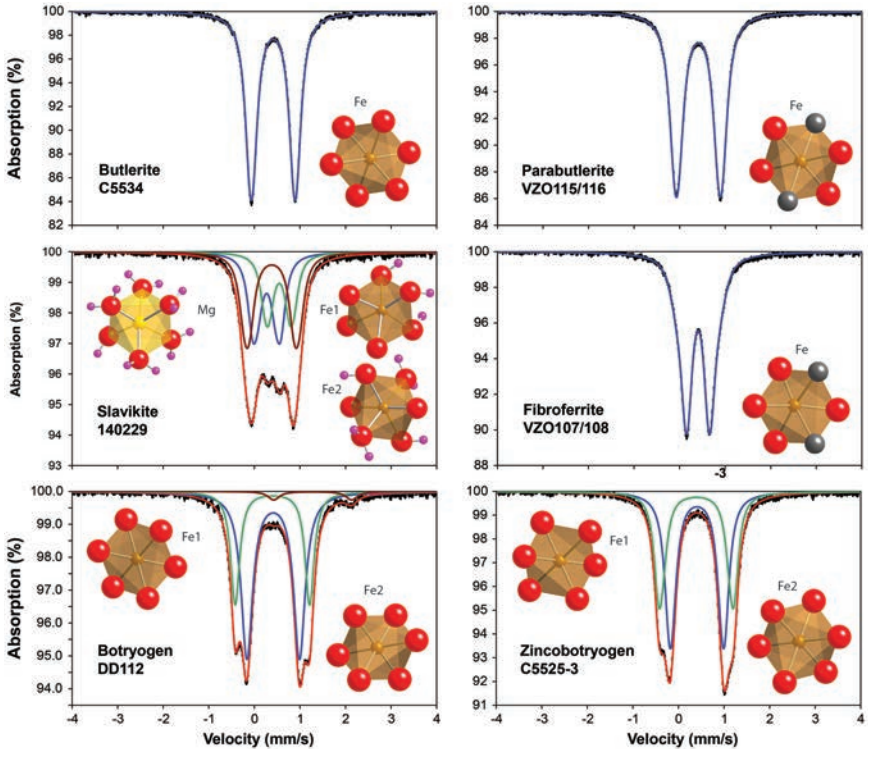

FIGURE 5. (**a**) Mössbauer spectra and Fe coordination polyhedra in sulfates with Δ values between ~0.80 and 1.12 mm/s. Polyhedra were created using CrystalMaker software and data from the American Mineralogist Crystal Structure Database: butlerite (Fanfani et al. 1971), parabutlerite (Borene 1970a), slavikite (Parafiniuk et al. 2010), fibroferrite (Scordari 1981), botryogen (Süsse 1967), and zincobotryogen (Süsse 1968a). O atoms are shown in red, OH in gray, H in pink, Mg in yellow, and Fe in orange. (Color online.)

(Continued on next page)

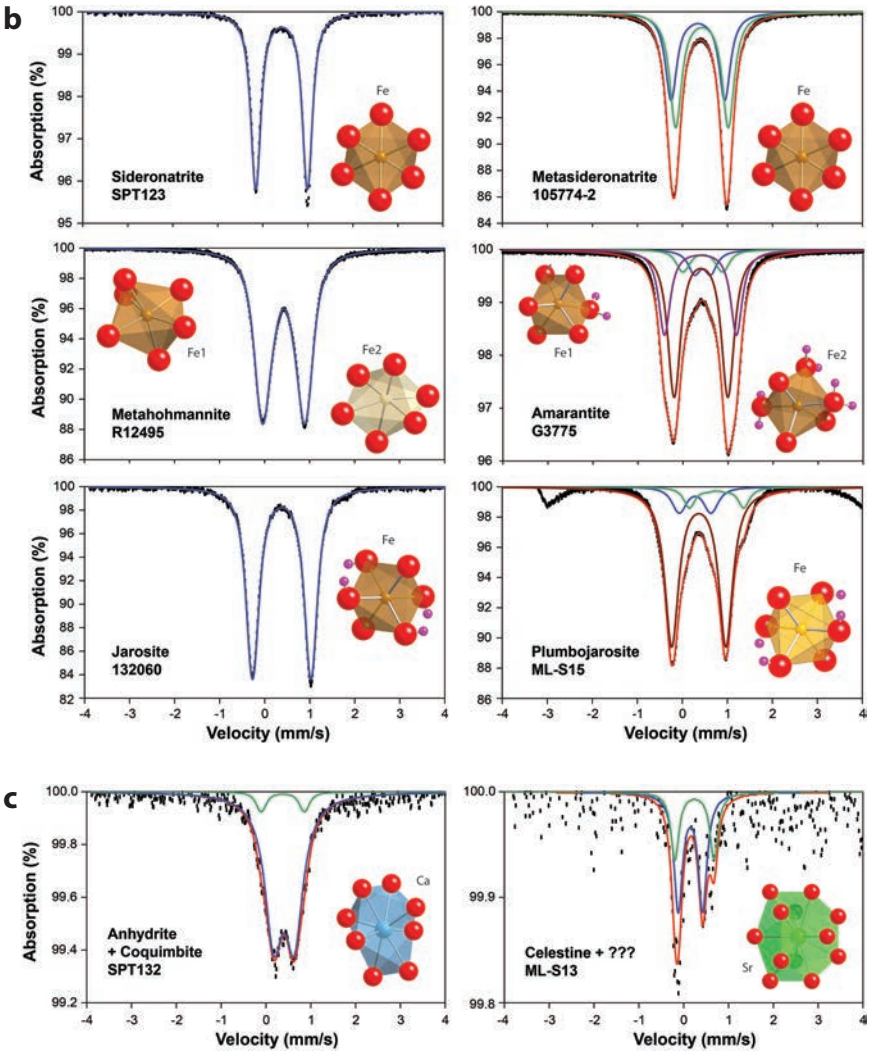

FIGURE 5.—*CONTINUED* (**b**) Mössbauer spectra and Fe coordination polyhedra in sulfates with Δ values between 0.94 and 1.22 mm/s. Polyhedra were created using CrystalMaker software and data from the American Mineralogist Crystal Structure Database: sideronatrite and metasideronatrite [Ventruti et al. (2010); metasideronatrite has the same structural unit topology as sideronatrite; Scordari and Ventruti (2009)], metahohmannite (Scordari et al. 2004), amarantite (Süsse 1968b), jarosite (Basciano and Peterson 2007), and plumbojarosite (Szymanski 1988). Note the presence of a magnetic phase impurity in plumbojarosite. O atoms are shown in red, H in pink, Mg in yellow, and Fe in orange. (**c**) Mössbauer spectra and Fe coordination polyhedra in sulfates without nominal Fe in their structures. Polyhedra were created using CrystalMaker software and data from the American Mineralogist Crystal Structure Database: anhydrite (Hawthorne and Ferguson 1975) and celestine (Miyake et al. 1978). O atoms are shown in red, Ca in blue, and Sr in green. Neither of these minerals is likely to contain much Fe because of the large size of the coordination polyhedra as seen here; these are configured to accommodate the Ca^{2+} cation, which is significantly larger than Fe^{3+}. Thus although the hand sample of SPT132 is mostly anhydrite, XRD reveals a significant component of coquimbite, which dominates the spectrum of the mixture because it is so much more Fe rich. Celestine ML-S13 is pure by XRD, but some Fe-rich phase is present there, too, at low concentrations. These data cannot discriminate between Fe in the celestine structure and Fe in an impurity. (Color online.)

There is no other closely related structure to voltaite among the sulfate minerals studied to date, so no similar Mössbauer parameters would be expected except as coincidence. Perhaps other species with frameworks of SO_4 tetrahedra and $Fe(H_2O)_6$ octahedra, as listed in Table 12 of Hawthorne et al. (2000), might have similar spectra. Small doublets with similar Mössbauer parameters were found in some of other spectra in this work. However, it is likely that these may represent small amounts of voltaite impurities—especially because the impurities occur in mineral species known to coexist with voltaite.

As noted in the earlier discussion of Fe^{3+} species, the structure of metavoltine contains isolated $[Fe^{2+}(H_2O)_6]$ octahedra in the Fe(3) site; there should be one Fe^{2+} for every ~six Fe^{3+} (Giacovazzo et al. 1976). Wet chemical analyses reported by Scordari (1975) suggest that Fe^{2+} in three different occurrences of metavoltine are only ~10% of the total Fe, with the balance

made up by Cu, Ni, Co, and Zn. Sample G2677 has 81% of the total Fe as Fe^{2+}, with doublet parameters of $\delta = 1.27$ mm/s and $\Delta = 3.23$ mm/s. These parameters are consistent with those observed by Sgarlata (1985).

None of the sulfates measured to date has significant Mössbauer doublets with quadrupole splittings between ~1.9 and 2.7 mm/s (Fig. 2). Above 2.70 mm/s, szomolnokite ($FeSO_4 \cdot H_2O$) is the Fe end-member of the six kieserite group minerals, which have butlerite-like chains cross-linked by sharing of corners between adjacent tetrahedra and octahedra. The Fe (and Mg, Mn, Cu, etc.) cations occupy octahedra with four corners shared with SO_4 and two with H_2O. Because they are isostructural, Fe^{2+} in all kieserite group phases (Fig. 1) would have the same or similar Mössbauer parameters. The main doublet in szomolnokite (Table 6; Fig. 6a) occurs at $\delta = 1.26$–1.31 mm/s and $\Delta = 2.73$–2.89 mm/s. Szmikite and gunningite spectra are similar to their szomolnokite relative, with a doublet with $\delta = 1.24$–1.25 mm/s and $\Delta = 2.59$–2.74 mm/s. These compare well with results of the many workers who have studied szomolnokite, including Van Alboom et al. (2009), Huggins and Huffman (1979), Montano (1981), Stiller et al. (1978), Russell and Montano (1978), and Giester et al. (1994). In general, these studies report Mössbauer parameters of $\delta = 1.18$–1.26 mm/s and $\Delta = 2.67$–2.71 mm/s for szomolnokite.

Of particular note is the work of Giester et al. (1994), who studied synthetic compositions along $FeSO_4 \cdot H_2O$–$CuSO_4 \cdot H_2O$ solid-solution series. They found values for $\delta = 1.24$–1.26 mm/s for $^{[M1]}Fe^{2+}$ and 1.35–1.25 mm/s for $^{[M2]}Fe^{2+}$, with $\Delta = 2.60$–2.71 mm/s for $^{[M1]}Fe^{2+}$ and 2.89–2.90 mm/s for $^{[M2]}Fe^{2+}$. Their work predicted a site preference of Cu^{2+} for the more distorted M1 octahedra, due to the Jahn-Teller effect. Their assignment of the lower-Δ doublet to M1 and the higher-Δ doublet to M2 was necessary to allow consistent interpretation of their cation ordering results and X-ray results. Although this trend is counter to what would be predicted by theory, it might represent a difference between sulfates and silicates. An alternate interpretation might be that differential recoil-free fractions on the two sites are giving anomalous doublet areas, complicating interpretation of their results.

However, those same parameters are also shared by other types of sulfate structures. The four chalcanthite group minerals, chalcanthite, siderotil, pentahydrite, and jokokuite, have solid solution between the species, and are closely related to their dehydration product, rozenite. They have formulas of $(Cu,Fe,Mg,Mn) \cdot 5H_2O$. Mössbauer spectra of chalcanthite ($\delta = 1.30$ mm/s and $\Delta = 2.88$ mm/s), pentahydrite ($\delta = 1.26$ mm/s and $\Delta = 3.00$ mm/s), and jokokuite ($\delta = 1.26$ mm/s and $\Delta = 3.00$ mm/s) as seen in Figure 6b are similar as expected, and reflect Fe^{2+} occupancy of octahedra linked to two SO_4 and four H_2O in corner-sharing chains.

Because halotrichite group minerals and römerite share very similar structures, the Mössbauer parameters of their Fe^{2+} doublets should be as similar as they were for Fe^{3+}, and this is again observed: $\delta_{Hal} = 1.28$ mm/s and $\Delta_{Hal} = 2.76$ mm/s, while $\delta_{Röm} = 1.26$–1.34 mm/s and $\Delta_{Röm} = 2.59$–2.78 mm/s. The Fe^{2+} doublets in the related species apjohnite and bilinite are slightly higher: $\delta_{Apj} = 1.27$ mm/s and $\Delta_{Apj} = 3.31$ mm/s, while $\delta_{Bil} = 1.06$ mm/s and $\Delta_{Bil} = 3.69$ mm/s (but note that the latter doublet is only 5% of the area in a dominantly Fe^{3+} sample, so the Fe^{2+} peaks are poorly resolved because they are so small).

Römerite also has a small doublet at $\delta = 1.24$ mm/s and $\Delta = 2.38$ mm/s, which probably represents Fe^{2+} in the isolated $[Fe^{2+}(H_2O)_6]$ octahedra (Fig. 1). Work by Huggins and Huffman (1979) found one Fe^{2+} doublet in römerite at $\delta = 1.27$ and $\Delta = 3.27$ mm/s (along with two Fe^{3+} doublets as mentioned in the preceding section), while Sgarlata (1985) observed $\delta = 1.31$ mm/s and $\Delta = 3.25$ mm/s for halotrichite.

The next higher hydration state above chalcanthite is the hexahydrite group of minerals $(Mg,Zn,Fe,Co,Ni,Mn)(SO_4) \cdot 6H_2O$, which is not represented in the currently studied suite of spectra. Their structures are composed of $M(H_2O)_6$ octahedra linked by weak hydrogen bonds to SO_4 tetrahedra. Their Mössbauer parameters would be predicted to be intermediate between those of chalcanthite and the melanterite group minerals, $(Fe,Cu,Zn,Co,Mn)(SO_4) \cdot 7H_2O$, because melanterite has a somewhat similar structure with only slightly higher $\Delta = 3.20$ mm/s (and $\delta = 1.27$ mm/s).

The probably isostructural melanterite group minerals melanterite ($Fe^{2+}SO_4 \cdot 7H_2O$), boothite, zinc-melanterite, bieberite, and mallardite are composed of isolated $M(H_2O)_6$ octahedra and SO_4 tetrahedra, again linked by hydrogen bonding (Fig. 1). This group is also structurally related to the epsomite group, which would be expected to have similar Mössbauer parameters. Melanterite 2070 in this study has parameters of $\delta = 1.27$ mm/s and $\Delta = 3.21$ mm/s, similar to those reported by Cheetham et al. (1981), Grant et al. (1966), Sakai et al. (1981), Montano (1981), Eissa et al. (1994a, 1994b), and Sallam et al. (1994) with a collective range of $\delta = 1.16$–1.31 mm/s and $\Delta = 3.17$–3.24 mm/s.

The isostructural rozenite group minerals [rozenite, $FeSO_4 \cdot (SO4) \cdot 4H_2O$, starkeyite, ilesite, aplowite, and boyleite] are based on clusters (cf. Anderson et al. 2012), which might suggest that their Mössbauer parameters should be similar to those of the halotrichite group. Each cluster is composed of two tetrahedra each sharing two corners with two octahedra; the resultant formula is $M_2(SO_4)_2O_8$, where M = Fe, Mg, Mn, Co, and/or Zn. Rozenite SPT130 has prameters of $\delta = 1.27$ mm/s and $\Delta = 3.21$ mm/s, comparable to those of the halotrichite group. Because they are isostructural, Fe^{2+} in all species within the rozenite group should have similar Mössbauer parameters. Parameters given in the literature for rozenite are $\delta = 1.23$–1.32 mm/s and $\Delta = 3.17$ mm/s (Montano 1981).

Relationships among coordination polyhedra geometries and Mössbauer parameters

As noted earlier, Mössbauer parameters are related to the geometries of the individual coordination polyhedra surrounding the Fe cations in each site. In particular, distortion of the octahedral environment may lead to unequal occupancy of the *d* orbitals and a large contribution to Δ from the electronic field. Thus, it should be possible to directly correlate Δ values with the characteristics of the octahedral sites in each mineral studied.

For this comparison, single-crystal structure refinements (SREF) of sulfate species were collected from the American Mineralogist Crystal Structure Database using data from the same species (though not the exact same samples) studied here. References to the SREF studies employed are given in captions

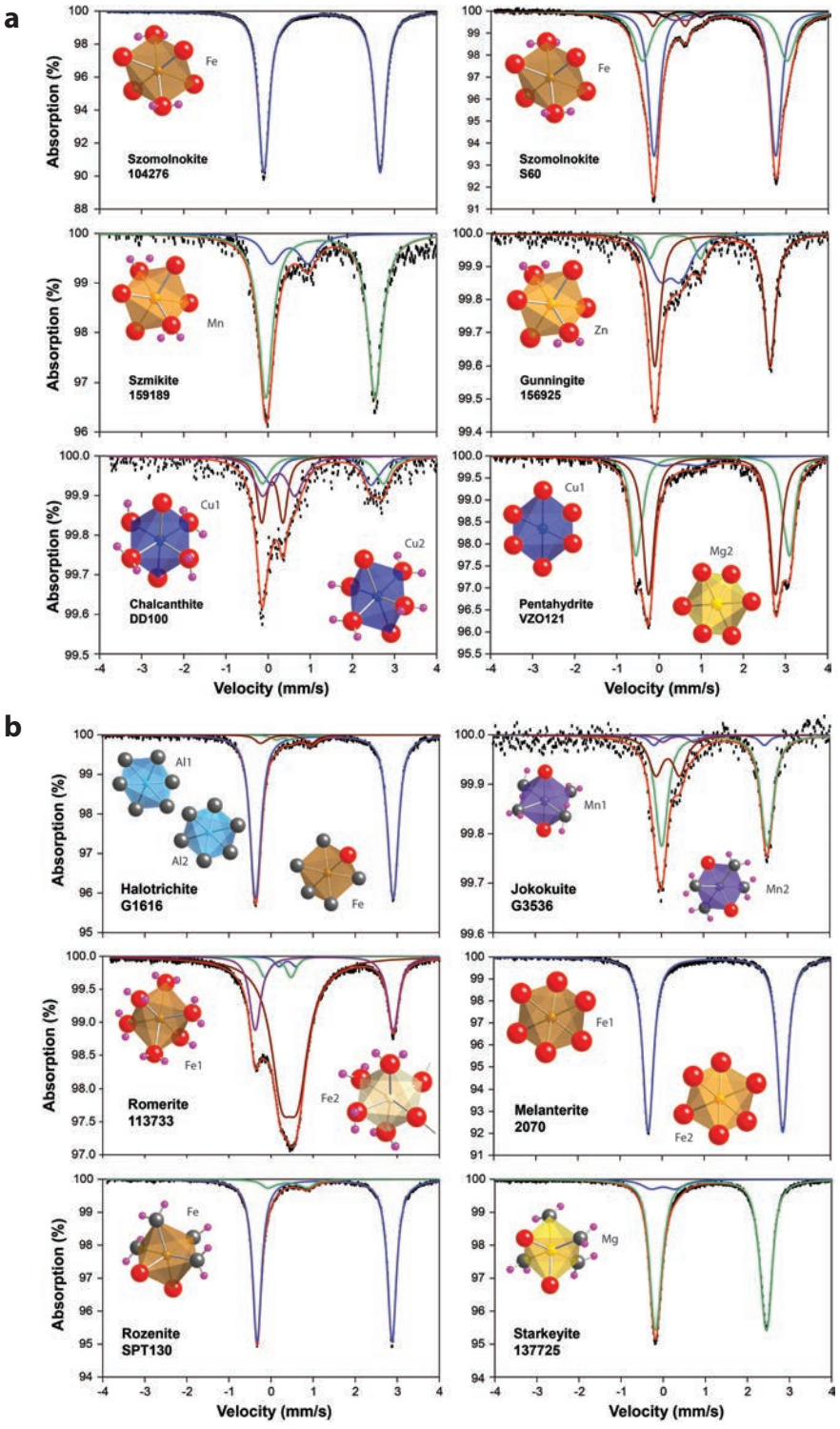

FIGURE 6. (a) Mössbauer spectra and Fe^{2+} coordination polyhedra in sulfates with Δ values larger than 2.70 mm/s. Polyhedra were created using CrystalMaker software and data from the American Mineralogist Crystal Structure Database: szomolnokite, szmikite, gunningite (Wildner and Giester 1991), chalcanthite (Bacon and Titterton 1975), and pentahydrite (Peterson et al. 2006). O atoms are shown in red, H in pink, Mg in yellow, Cu in purple, and Fe and Zn in orange. (**b**) Mössbauer spectra and Fe^{2+} coordination polyhedra in sulfates with highest Δ values. Polyhedra were created using CrystalMaker software and data from the American Mineralogist Crystal Structure Database: halotrichite (Lovas 1986), jokokuite (Caminiti et al. 1982), römerite (Fanfani et al. 1970), melanterite (Peterson 2003), rozenite (Baur 1962), and starkeyite (Baur 1962). O atoms are shown in red, OH in gray, H in pink, Mg in yellow, Al in blue, and Fe in orange. (Color online.)

to Figures 3 to 6. Using those crystal structure data and the CrystalMaker software package, parameters describing the six-coordinated sites in each of the sulfates studied (except bilinite, for which no refinement has been published) were evaluated. On the basis of the atomic coordinates, calculated mean bond length, mean octahedral quadratic elongation (λ), and angular variance (σ) of each cation site where Fe may reside in these minerals were calculated. The latter two parameters were devised by Robinson and Fang (1971) to summarize variations in bond length and bond angle. The quadratic elongation parameter (λ) provides a quantitative measurement of polyhedral distortion that is independent of polyhedral size

$$\lambda = \sum_{i=1}^{n} \left(\frac{l_i}{l_0} \right)^2 / n \quad (1)$$

where l_i is the measured bond distance (where $n = 6$ for 6-coordination) and l_0 is the bond distance in a perfect (undistorted, equal volume) octahedron. Angular variance (σ) is calculated using the expression

$$\sigma = \sum_{i=1}^{n} \left(\theta_i - \theta_{\text{avg}} \right)^2 / (n-1) \quad (2)$$

where θ_i is the measured angle in the crystal structure (there are $n = 12$ angles in a six-coordinated site) and θ_{avg} is the bond angle for a perfect octahedron (all angles are 90°). These structural data were compared with Δ values for the samples studied. In cases where there are multiple sites possible for Fe atoms, Mössbauer doublets were assigned on the basis of consistency with related structures and relative distortion. Refinements where the composition was low in Fe were not used, because those site characteristics are more reflective of the other cation than of Fe occupancy. The refinement of apjohnite by Menchetti and Sabelli (1976) was not used because its parameters lay far off the trends of all other samples, suggesting a possible problem with the Crystallographic Interchange File (CIF) format.

Results of these comparisons are shown for Fe^{3+} in Figure 7. The plot of angular variance shows no systematics with Δ, but the other polyhedral parameters show some interesting trends despite the varying quality and sophistication of the structure refinements. There is an increase in quadrupole splitting with octahedral volume and mean bond length. Quadratic elongation decreases slightly with increasing Δ. This observation may seem counter to the assumption that Δ generally increases with distortion, but λ is just one of the possible formulations that could be used to describe that distortion and λ is also insensitive to polyhedral size. No trend is seen for angular variance. Thus it appears that for sulfate minerals, the best predictor of quadrupole splitting (and thus peak location) is the size of the coordination polyhedron in any given mineral species. Comparable plots for Fe^{2+} are not shown because there are only a few data points and they all fall within two small groups of quadrupole splitting.

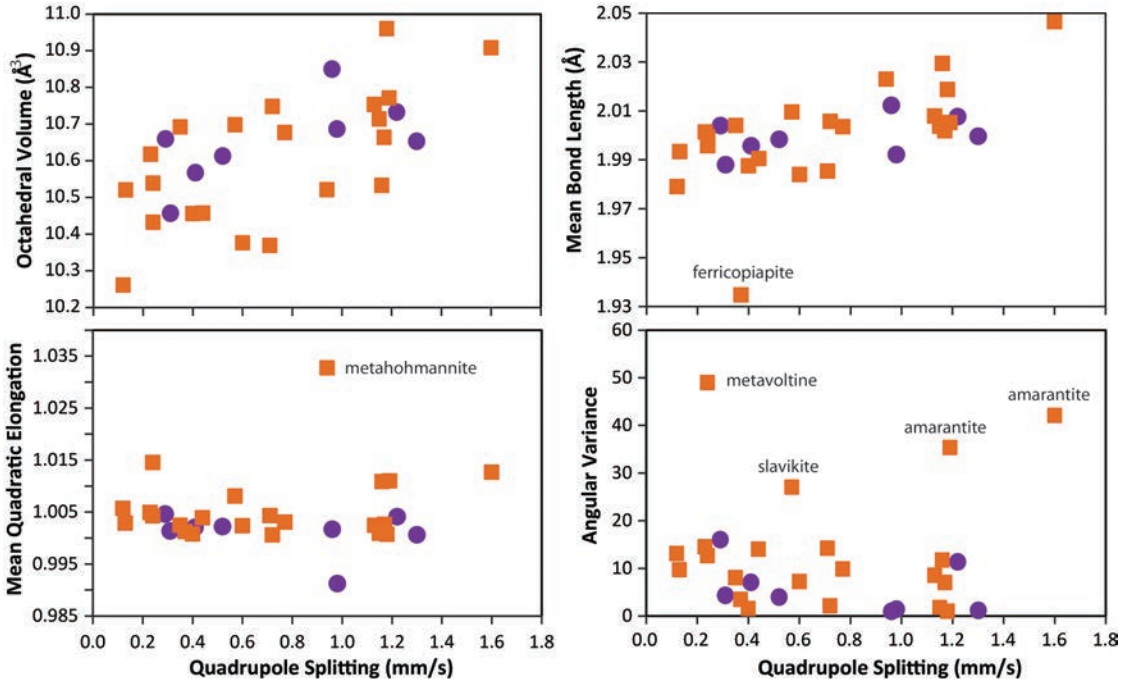

FIGURE 7. Quadruple splitting plotted against various characteristics of the geometry of the Fe^{3+} coordination polyhedra: octahedral volume, mean octahedral bond length, mean quadratic elongation, and angular variance. See text for definitions. Purple circles represent parameters of structures with only one possible Fe cation site. Orange squares are mineral species in which Fe occupies more than one site; Mössbauer parameters were matched with sites by inspection. Error bars are ±0.03–0.05 mm/s for quadruple splitting and highly variable for the structure refinements, depending on the accuracy of the original measurements. The few labeled outliers are so far out of range from the majority of the measurements that they may likely be attributed to problems with the original refinements or their transcription into CIF files. The parameters for Fe^{2+} sites are not shown because there are too few data points and the parameters group together in two clumps. (Color online.)

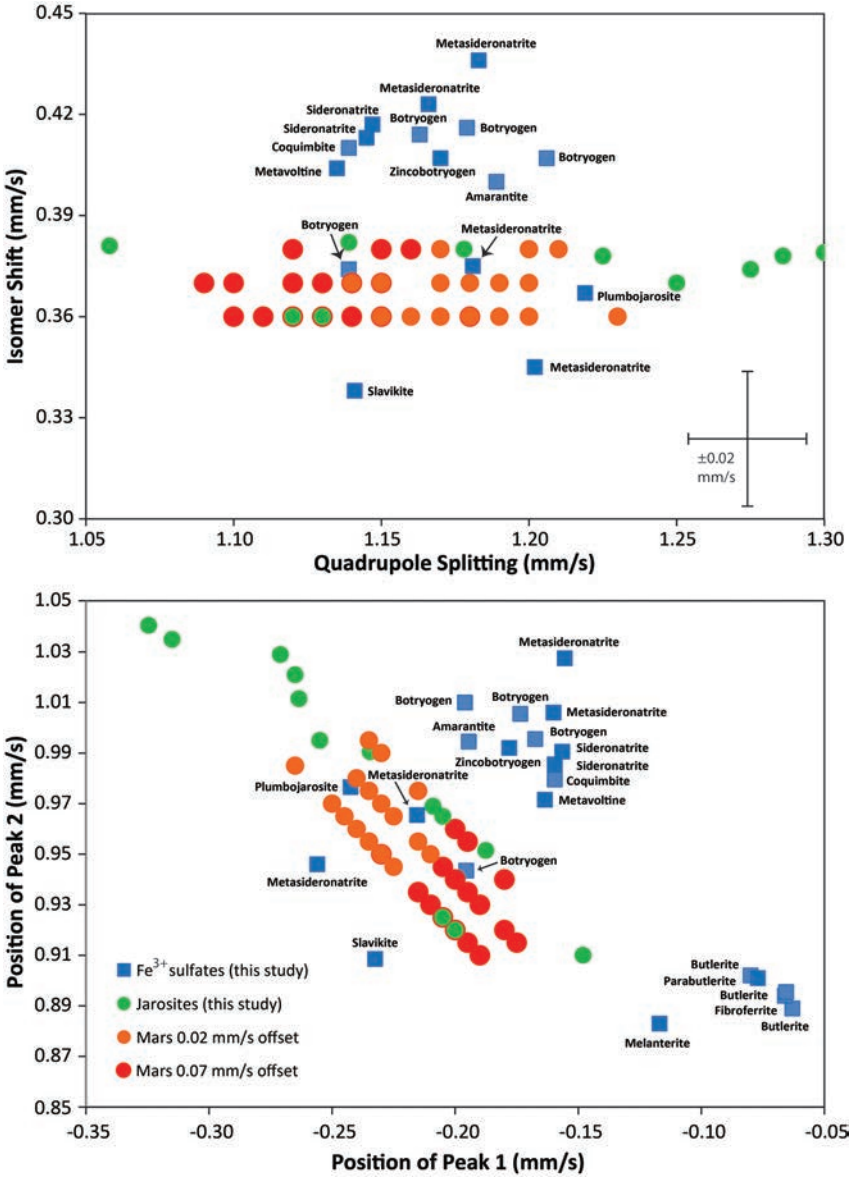

FIGURE 8. Mössbauer parameters of several sulfates with very similar peak positions (close-up of Fig. 2). Blue squares represent Fe^{3+}-bearing sulfates from this study, not including jarosites. Green circles are jarosite data from this study. Circles display parameters and locations for Mars data from Morris et al. (2006) offset by –0.07 or –0.02 mm/s to correct Mars data to room temperature. The error bar for both plots is shown at lower right in upper panel. (Color online.)

Implications: Uniqueness of sulfate Mössbauer parameters

As noted at the onset, the MIMOS II Mössbauer spectrometers on the Mars Exploration Rovers identified jarosite at the Meridiani Planum landing site based on the presence of a peak with $\Delta = 1.22$ mm/s at $T = 240 \pm 40$ K. Errors on the Mars fit parameters are quoted as ±0.02 mm/s. The same Mars spectra were also fit using the software from the current study (Dyar et al. 2006c), resulting in more variability in peak positions, with $\delta = 0.28$–0.41 and $\Delta = 1.19$–1.27 mm/s. The extrapolation of the low and variable temperature to 295 K was estimated by Klingelhöfer et al. (2004) to be –0.07 mm/s, although Rothstein (2006) found only a –0.02 mm/s offset in laboratory spectra. In any case, based on the data available to them in 2004, the team assigned that doublet to jarosite, later suggested to be hydronium jarosite (Morris et al. 2007). Results from the current study (blue squares and green circles) are plotted with the Mars data (orange and red circles) in Figure 8, and support the assignment to jarosite but show that many sulfate minerals have parameters close to those of jarosites, as measured under optimal laboratory conditions with state of the art equipment, including botryogen, metasideronatrite, slavikite, etc. A small deviation in peak position of the Mars data could easily result in overlap with many different possible sulfate mineral species. As seen in Figure 9, the Fe polyhedra in these sulfates are strikingly similar, so it is not

surprising that the Mössbauer peaks should be so similar as well.

At the Gusev Crater site, there are two different features that might be assigned to Fe^{3+} sulfate. The first is a doublet designated Fe3D1, which is assigned by Morris et al. (2008) to a generic Fe^{3+} alteration product nanophase Fe oxide, although Morris et al. (2007) suggest that the higher Δ doublets in that range might be attributed to hydronium jarosite. The parameters of the Fe3D1 doublet do not overlap with those from any of the Fe^{3+} sulfates from this paper, in support of the assignment to nanophase Fe oxides. The second feature noted by Morris et al. (2008) is assigned to a Fe^{3+} sulfate designated as Fe3D2 (Fig. 10) that is not specified. On the basis of the current study, optimal candidates for the feature at Arad Samra would be fibroferrite and rhomboclase and likely copiapite or parabutlerite at Tyrone Mount Darwin and Berkner Island (Fig. 10). It must be stressed, however, that such assignments presume that the phase in question is one of those studied here, and that it is indeed a sulfate.

In making these conclusions, it is important to note the importance of independent corroboration from other techniques, without which Mössbauer results cannot be used to distinguish sulfates from other common Fe^{3+}-bearing phases (even sulfides). The current study was focused on hydrous sulfates, and sample selection was biased in that direction. However, there are other sulfate, sulfide, and S-containing minerals that should be considered as candidates for Mars. For example, the related phase schwertmannite [$Fe^{3+}_{16}O_{16}(OH)_{12}(SO_4)_2$] is formally considered to be a hydroxide containing hydroxyl (Dana class 6). Mössbauer spectra of schwertmannite have been extensively studied by many workers, including Bigham et al. (1994), Schwertmann et al. (1995), Bishop and Murad (1996), and Bigham and Murad (1997). Typical parameters are δ = 0.37 mm/s and Δ = 0.61–0.81 mm/s, which overlap with those of other hydrous Fe^{3+} sulfates discussed above. Mössbauer spectra of sulfide minerals also overlap with several species in this study, including pyrite (Silva et al. 2011: δ = 0.27–0.30 and Δ = 0.55–0.62 mm/s) and sphalerite (unpublished data: δ = 0.30 mm/s and Δ = 0.46 mm/s).

For Fe^{2+} sulfates, identification on the basis of Mössbauer spectra is complicated by the potential for overlap with olivine

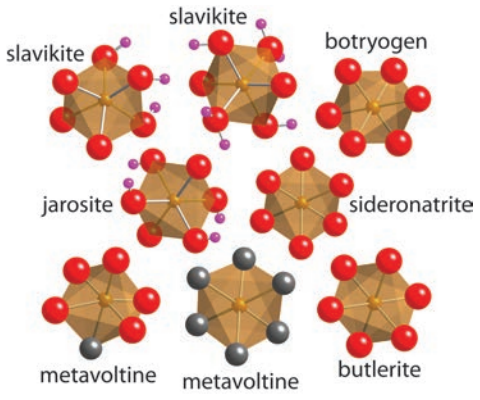

FIGURE 9. Comparison of the crystal structures surrounding the Fe^{3+} cations in several sulfates that have similar Mössbauer spectra (see Fig. 8). Red spheres represent O^{2-}, gray are OH^-, pink are H^+, and the central gold cations are Fe^{3+}. Note that both slavikite (Fe1 at upper left, and Fe2 at top center) and metavoltine (Fe^{3+}1,2 at lower left and Fe^{2+}3 at bottom center) have multiple different Fe sites with slightly differing geometries. (Color online.)

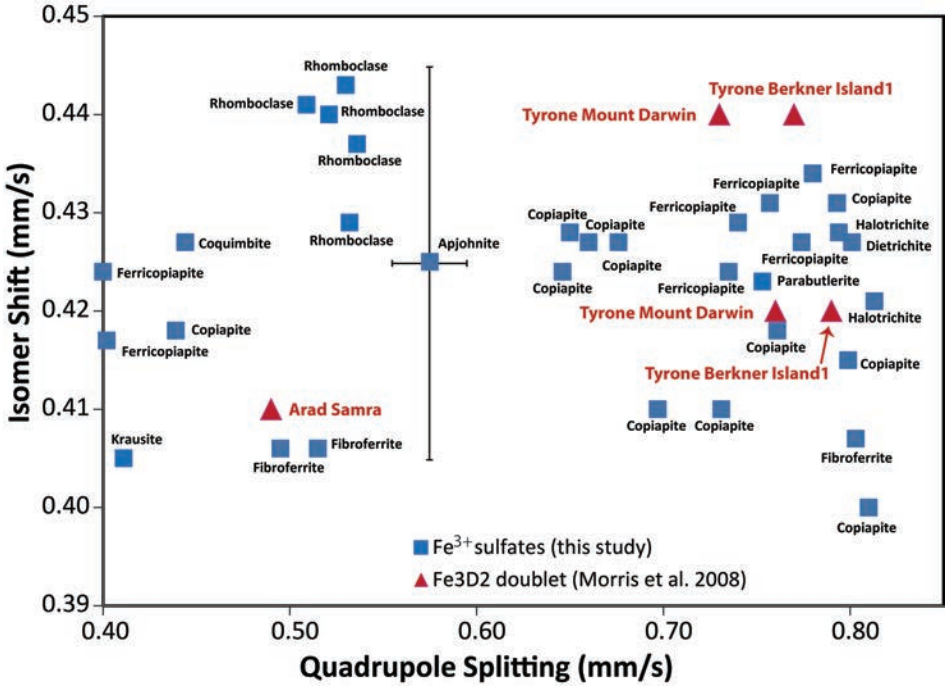

FIGURE 10. Mössbauer parameters of several sulfates with very similar peak positions (close-up of Fig. 2). Blue squares represent Fe^{3+}-bearing sulfates from this study. Red triangles are data from Mars (Morris et al. 2008) using a temperature-correcting offset of –0.07 mm/s. The error bar shown for apjohnite applies to all samples. (Color online.)

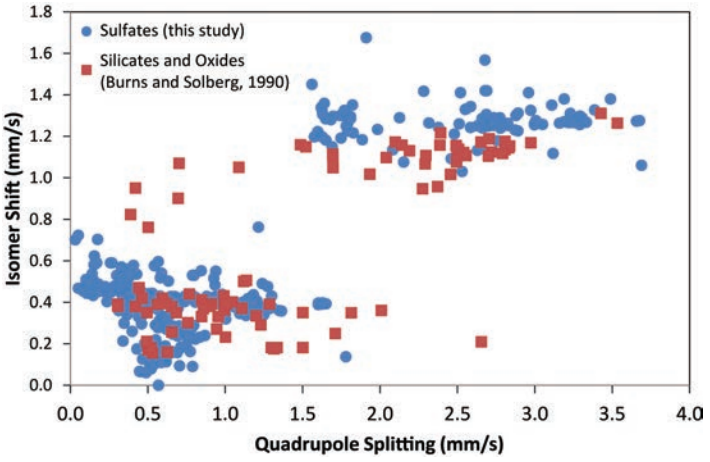

◀**FIGURE 11.** Mössbauer data from this study (blue circles) with data for silicates and oxides from Burns and Solberg (1990) superimposed. These results highlight the small range of Mössbauer parameters that occur in minerals, and underscore the non-uniqueness of the parameters to specific mineral groups. (Color online.)

peaks (Lane et al. 2004). The range of measured Mössbauer parameters for Fe^{2+} in synthetic olivines has been well studied (Sklute et al. 2005; Sklute 2006): δ = 1.13–1.17 mm/s and Δ = 2.80–3.05 mm/s. Fe^{2+} sulfates (Table 6) have comparable Δ but higher δ values (ca. 1.25–1.33 mm/s), allowing olivine to be distinguished from Fe^{2+} sulfates under optimal experimental conditions. When these parameters are converted to peak positions, it is apparent that an error of 0.1 mm/s in velocity would be enough to make sulfates and olivines indistinguishable.

This discussion highlights both the strengths and weaknesses of Mössbauer spectroscopy. Highly reproducible spectra can be acquired under a range of conditions and instrument geometries from transmission to backscatter mode, in the laboratory or on the surface of Mars. Species within groups of naturally occurring minerals have spectral peaks that generally fall within small velocity ranges. Spectral parameters can be qualitatively related to the geometries of the individual Fe coordination polyhedra. In cases where independent constraints on phase identity are available, this capability allows Mössbauer spectroscopy to assist in understanding the distribution of Fe and its valence states among different coexisting phases. On Mars, the MIMOS spectrometers were pressed into service for mineral identification in conjunction with bulk chemical results from the α particle X-ray spectrometer instrument and deductions based on phase equilibria of likely martian assemblages. The success of the MER missions owes much to constraints placed on mineral identification by the Mössbauer spectrometers based on comparisons to contemporary databases of spectra.

However, for paramagnetic minerals, it must be acknowledged that the range of Mössbauer parameters is small (particularly for Fe^{3+}), and many phases have overlapping parameters (Fig. 11). For example, Fe^{2+} doublets in orthopyroxene will be unrecognizable from Fe^{2+} in clinopyroxene (Dyar et al. 2013) and analogous to several different Fe^{3+} sulfates (among many other possibilities). Pyroxene, amphibole, and mica (including clay mineral) spectra will be generally indistinguishable because the structures are all so similar. In other words, the number of mineral species is large and the range of hyperfine parameters is small, so that in many cases, phases cannot be uniquely identified. This is particularly true for Fe^{3+}-rich phases, because the absolute range of Mössbauer parameters for Fe^{3+} in any coordination number is so small.

Evaluating the crystal structures of these minerals provides explanations for the similarities in Mössbauer parameters. Because mineral structures based on varying linkages among tetrahedra are universal (cf. Fig. 1), silicate and sulfate (and phosphate, perchlorate, etc.) structures will have much in common. The resultant octahedral sites between those tetrahedra will occur in various geometries, but crystal chemistry shows that many groups will be similar because their structural frameworks are the same. In turn, Fe cations in those similar crystallographic sites will give rise to Mössbauer doublets with comparable parameters, and thus the range of observed Mössbauer parameters is relatively small for most minerals. For this reason, Mössbauer spectroscopy is rarely used in terrestrial labs for mineral identification because so many other more appropriate techniques are widely available (e.g., X-ray diffraction). The true strength of the Mössbauer technique lies in its ability to measure valence states and site occupancies of Fe and identify magnetic phases. This study shows that Mössbauer data can also inform our understanding of the local environment around the Fe polyhedra, and thus provide distinctions among different phases that, when combined with other types of information, can assist with mineral identification even in paramagnetic materials.

ACKNOWLEDGMENTS

We are grateful to Ed Cloutis, the Harvard Mineralogical Museum, and the NMNH for the loan of samples, and for support from NSF grants EAR-043907 and EAR-0439161 and NASA grants NNG04GG12G, NAG5-12687, and NNX-11AF11G. Student support for this project was provided by the Massachusetts Space Grant Consortium. Thoughtful suggestions from two anonymous reviewers and Juraj Majzlan were greatly appreciated. We thank David Palmer for help with the CrystalMaker models. This is PSI Contribution Number 605.

REFERENCES CITED

Afanasev, A.M., Gorobchenko, V.D., Kulgawczuk, D.S., and Lukashevich, I.I. (1974) Nuclear γ-resonance in iron sulphates of the jarosite group. Physica status solidi (a), 26, 697–701.

Ahmed, M.A., Vandenberghe, R.E., De Grave, E., Eissa, N.A., and Ibarra, J.V. (1999) Characterisation of Spanish coal by means of Mössbauer spectroscopy. Fuel, 78, 453–457.

Ahmed, M.A., Blesa, M.J., Juan, R., and Vandeberghe, R.E. (2003) Characterization of an Egyptian coal by Mössbauer and FT-IR spectroscopy. Fuel, 82, 1825–1829.

Anderson, J.L., Peterson, R.C., and Swainson, I. (2012) The atomic structure of deuterated boyleite $ZnSO_4{\cdot}4D_2O$, ilesite $MnSO_4{\cdot}4D_2O$, and bianchite $ZnSO_4{\cdot}6D_2O$. American Mineralogist, 97, 1905–1914.

Audley, G.J., Pyne, G.S., Tricker, M.J., Cranshaw, T.E., and Laundy, B.J. (1986) A new approach to the determination of pyrite in coals by Mössbauer spectroscopy. Fuel, 65, 1103–1107.

Bacon, G.E., and Titterton, D.H. (1975) Neutron-diffraction studies of $CuSO_4{\cdot}5(H_2O)$ and $CuSO_4{\cdot}5(D_2O)$. Zeitschrift für Kristallographie, 141, 330–341.

Ballirano, P., Bellatreccia, F., and Grubessi, O. (2003) New crystal-chemical and structural data of dietrichite, ideally $ZnAl_2(SO_4)_4{\cdot}22H_2O$, a member of the halotrichite group. European Journal of Mineralogy, 15, 1043–1049.

Basciano, L.C., and Peterson, R.C. (2007) Jarosite-hydronium jarosite solid solution series with full iron occupancy: Mineralogy and crystal chemistry. American Mineralogist, 92, 1464–1473.

Baur, W.H. (1962) Zur kristallchemie der salzhydrate. Die kristallstrukturen von $MgSO_4{\cdot}4H_2O$ (leonhardtit) und $FeSO_4{\cdot}4H_2O$ (rozenit). Acta Crystallographica, 15, 815–826.

Berlepsch, P., Armbruster, T., Brugger, J., Bykova, E.Y., and Kartashov, P.M. (1999) The crystal structure of vergasovaite $Cu_3O[(Mo,S)O_4SO_4]$ and its relation to synthetic $Cu_3O[MoO_4]_2$. European Journal of Mineralogy, 11, 101–110.

Bigham, J.M., and Murad, E. (1997) Mineralogy of ocher deposits formed by the oxidation of iron sulfide minerals. In K. Auerswald, H. Stanjek, and J.M. Bigham, Eds., Advances in GeoEcology, 35447, pp. 193–225. Catena Verlag, Reiskirchen, Germany.

Bigham, J.M., Carlson, L., and Murad, E. (1994) Schwertmannite: A new iron oxyhydroxysulphate from Pyhasalmi, Finland, and other localities. Mineralogical Magazine, 58, 641–648.

Bishop, J.L., and Murad, E. (1996) Schwertmannite on Mars? Spectroscopic analyses of schwertmannite, its relationship to other ferric minerals, and its possible presence in the surface material on Mars. In mineral spectroscopy: A tribute to Roger G. Burns, Geochemical Society Special Publication, 5, 337–358.

Blake, D., Vaniman, D., Achilles, C., Anderson, R., Bish, D., Bristow, T., Chen, C., Chipera, S., Crisp, J., Des Marais, D., and others. (2012) Characterization and calibration of the CheMin mineralogical instrument on Mars Science Laboratory. Space Science Reviews, 170, 341–399.

Blaney, D.L., and McCord, T.B. (1995) Indications of sulfate minerals in the Martian soil from Earth-based spectroscopy. Journal of Geophysical Research, 100, 14433–14441.

Bonello, G., Bibring, J.P., Poulet, F., Gendrin, A., Gondet, B., Langevin, Y., and Fonti, S. (2004) Visible and infrared spectroscopy of minerals and mixtures with the OMEGA-Mars-EXPRESS instrument. Planetary and Space Sciences, 52, 133–140.

Borene, J. (1970) Structure cristalline de la parabutlerite. Bulletin de la Societe Francaise de Mineralogie et de Cristallographie, 93, 185–189.

Bregeault, J., Herpin, P., Manoli, J., and Pannetier, G. (1970) Affinement de la structure de la kieserite $Mg(SO_4)$ (H_2O). Bulletin de la Societe Chimique de France, 4243–4248.

Brigatti, M.F., Gali, E., and Medici, L. (1997) Ba-rich celestine: New data and crystal structure refinement. Mineralogical Magazine, 61, 447–451.

Burns, R.G. (1986) Terrestrial analogues of the surface rocks of Mars? Nature, 320, 55–56.

——— (1987) Ferric sulfates on Mars. Proceedings of the Lunar and Planetary Science Conference, 17, Part 2. Journal of Geophysical Research, 92, suppl., E570–E574.

——— (1988) Gossans on Mars. Proceedings of the Lunar and Planetary Science Conference, 18, 713–721.

——— (1993) Rates and mechanisms of chemical weathering of ferromagnesian silicate minerals on Mars. Geochimica et Cosmochimica Acta, 57, 4555–4574.

Burns, R.G., and Fisher, D.S. (1990) Evolution of sulfide mineralization on Mars. Journal of Geophysical Research, 95, 14169–14173.

Burns, R.G., and Solberg, T.C. (1990) ^{57}Fe-bearing oxide, silicate, and aluminosilicate minerals, crystal structure trends in Mossbauer spectra, in Spectroscopic characterization of minerals and their surfaces, 415, pp. 262–283. American Chemical Society Symposium Series, Washington, D.C.

Caminiti, R., Marongiu, G., and Paschina, G. (1982) A comparative X-ray diffraction study of aqueous $MnSO_4$ and crystals of $MnSO_4{\cdot}5H_2O$. Zeitschrift für Naturforschung, A37, 581–586.

Cheetham, A.K., Cole, A.J., and Long, G.J. (1981) Investigation of the mixed-metal sulfide $(Mn,Fe)S_2$ by analytical electron microscopy and Mössbauer spectroscopy. Inorganic Chemistry, 20, 2747–2750.

Clark, B.C., Baird, A.K., Welcon, R.J., Tsusaki, D.M., Schnabel, L., and Candelaria, M.P. (1982) Chemical composition of Martian fines. Journal of Geophysical Research, 87, 10059–10067.

DeBenedetti, S., Lang, G., and Ingalls, R. (1961) Electric quadrupole splitting and the nuclear volume effect in the ions of Fe^{57}. Physical Review Letters, 6, 60–62.

Duesler, E.N., and Foord, E.E. (1986) Crystal structure of hashemite, $BaCrO_4$, a barite structure type. American Mineralogist, 71, 1217–1220.

Dyar, M.D. (1984) Precision and interlaboratory reproducibility of measurements of the Mössbauer effect in minerals. American Mineralogist, 69, 1127–1144.

Dyar, M.D., Agresti, D.G., Schaefer, M., Grant, C.A., and Sklute, E.C. (2006a) Mössbauer spectroscopy of earth and planetary materials. Annual Reviews of Earth and Planetary Science, 34, 83–125.

Dyar, M.D., Podratz, L., Sklute, E.C., Rusu, C., Rothstein, Y., Tosca, N., Bishop, J.L., and Lane, M.D. (2006b) Mössbauer spectroscopy of synthetic alunite group minerals. Workshop on Martian Sulfates as Recorders of Atmospheric-Fluid-Rock Interactions, no.7053.

Dyar, M.D., Rothstein, Y., Schaefer, M.W., and Agresti, D. (2006c) Mössbauer spectroscopy of outcrop at the Merdiani Planum site. Lunar and Planetary Science XXXVII, Abstract no. 2382.

Dyar, M.D., Schaefer, M.W., Sklute, E.C., and Bishop, J.L. (2008) Mössbauer spectroscopy of phyllosilicates: Effects of fitting models on recoil-free fractions and redox ratios. Clay Minerals, 43, 3–33.

Dyar, M.D., Klima, R.L., Fleagle, A., and Peel, S.E. (2013) Fundamental Mössbauer parameters of synthetic Ca-Mg-Fe pyroxenes. American Mineralogist, 98, 1172–1186.

Eissa, N.A., Sheta, N.H., El-Mossallamy, S.M., Soliman, M.A., and El-Fouly, M.H. (1994a) Study of the dehydration process of melanterite under heat treatment and gamma irradiation effects using Mössbauer spectroscopy and thermal analysis measurements. Arab Journal of Nuclear Sciences and Applications, 27, 33–45.

Eissa, N.A., Sallam, H.A., Sheta, N.H., Radwan, Sh.N., and Soliman, M.A. (1994b) Mössbauer study of the role of Fe^{2+}/Fe^{3+} ratio and water of hydration on the optical and electrical properties of gamma-irradiated melanterite. Arab Journal of Nuclear Sciences and Applications, 27, 143–154.

Eneroth, E., and Koch, C.B. (2004) Fe-Hydroxysulphates from bacterial Fe^{2+} oxidation. Hyperfine Interactions, 156, 423–429.

Ertl, A., Dyar, M.D., Hughes, J.M., Brandstätter, F., Gunter, M., Prem, M., and Peterson, R.C. (2008) Pertlikite, a new netragonal Mg-rich member of the voltaite group from Madeni Zakh, Iran. Canadian Mineralogist, 46, 661–669.

Fajardo, M., Mojica, J., Barraza, J., Perez Alcazar, G.A., and Tabares, J.A. (1999) Mineral identification in Colombian coals using Mössbauer spectroscopy and X-ray diffraction. Hyperfine Interactions, 122, 129–138.

Fanfani, L., Nunzi, A., and Zanazzi, P.F. (1970) The crystal structure of römerite. American Mineralogist, 55, 78–89.

——— (1971) The crystal structure of butlerite. American Mineralogist, 56, 751–757.

Fanfani, L., Nunzi, A., Zanazzi, P.F., and Zanzari, A.R. (1973) The copiapite problem: The crystal structure of a ferrian copiapite. American Mineralogist, 58, 314–322.

Fang, J.H., and Robinson, P.D. (1970) Crystal structures and mineral chemistry of hydrated ferric sulfates. I. The crystal structure of coquimbite. American Mineralogist, 55, 1534–1540.

Fernández-Remolar, D.C., Morris, R.V., Gruener, J.E., Amils, R., and Knoll, A.H. (2005) The Río Tinto Basin, Spain: Mineralogy, sedimentary geobiology, and implications or interpretation of outcrop rocks at Meridiani Planum, Mars. Earth and Planetary Science Letters, 240, 149–167.

Gancedo, J.R., Gracia, M., Martinez-Alonso, A., Miranda, J.L., and Tascon, J.M.D. (1992) Mössbauer study of the effect of acidic treatment on iron minerals during the demineralization of coals. Hyperfine Interactions, 71, 1403–1406.

Giacovazzo, C., Scordari, F., Todisco, A., and Menchetti, S. (1976) Crystal structure model for metavoltine from Sierra Gorda. Tschermaks Mineralogische und Petrographische Mitteilungen, 23, 155–166.

Giester, G., Lengauer, C.I., and Redhammer, G. (1994) Characterization of the $FeSO_4{\cdot}H_2O$-$CuSO_4{\cdot}H_2O$ solid solution series and the nature of poitevinite, $(Cu,Fe)SO_4{\cdot}H_2O$. The Canadian Mineralogist, 32, 873–884.

Gracia, M., Gancedo, J.R., Martinez-Alonso, A., and Tascon, J.M.D. (1990) Comparative Mössbauer study of the oxidation of pyrite under different conditions. Hyperfine Interactions, 58, 2581–2588.

Graeber, E.J., and Rosenzweig, A. (1971) The crystal structures of yavapaiite, $KFe(SO_4)_2$, and goldichite, $KFe(SO_4)_2 4H_2O$. American Mineralogist, 56, 1917–1933.

Graeber, E.J., Morosin, B., and Rosenzweig, A. (1965) The crystal structure of krausite, $KFe(SO_4)_2{\cdot}H_2O$. American Mineralogist, 50, 1929–1936.

Grant, R.W., Wiedersich, H., Muir, A.H. Jr., Gonser, U., and Delgass, W.N. (1966) Sign of the nuclear quadrupole coupling constants in some ionic ferrous compounds. The Journal of Chemical Physics, 45, 1015–1019.

Grinkevich, A.Z., and Kul'gavchik., D.S. (1963) The fine structure of Mössbauer spectra in mineral compounds of iron. Proceedings of the Dubna Conference on the Mössbauer Effect, 18-EOA.

Hawthorne, F.A. (1985) Toward a structural classification of minerals: the $^{VI}M^{IV}T_2\Phi_n$ minerals. American Mineralogist, 70, 455–473.

Hawthorne, F.C. (1979) The crystal structure of morinite. Canadian Mineralogist, 17, 93–102.

Hawthorne, F.C., and Ferguson, R.B. (1975) Anhydrous sulphates. II. Refinement of the crystal structure of anhydrite. The Canadian Mineralogist, 13, 289–292.

Hawthorne, F.C., Krivovichev, S.V., and Burns, P.C. (2000) The crystal chemistry of sulfate minerals. In C.N. Alpers, J.L. Jambor, and D.K. Nordstrom, Eds., Sulfate minerals: Crystallography, Geochemistry, and Environmental Significance, 40, 1–112. Reviews in Mineralogy and Geochemistry, Mineralogical Society of America, Chantilly, Virginia.

Held, P., and Bohaty, L. (2002) Manganese(II) sulfate tetrahydrate (ilesite). Acta Crystallographica, E58, i121–i123.
Herbert, R.B.J. (1997) Properties of goethite and jarosite precipitated from acidic groundwater, Dalarana, Sweden. Clays and Clay Minerals, 45, 261–273.
Hermon, E., Haddad, R., Simkin, D., Brandão, D.E., and Muir, W.B. (1976) Magnetic properties and the distribution of iron ions in voltaites. Canadian Journal of Physics, 54, 1149–1156.
Herzenberg, C.L., and Toms, D. (1966) Mössbauer absorption measurements in iron-containing minerals. Journal of Geophysical Research, 71, 2661–2677.
Hrynkiewicz, A.Z., Kubisz, J., and Kulgawczuk, D.S. (1965) Quadrupole splitting of the 14.4 keV gamma line of ^{57}Fe in iron sulphates of the jarosite group. Journal of Inorganic Nuclear Chemistry, 27, 2513–2517.
Huggins, F.E., Huffman, G.P., and Lin, M.C. (1983) Observations on low-temperature oxidation of minerals in bituminous coals. International Journal of Coal Geology, 3, 157–182.
Huggins, G.P., and Huffman, F.E. (1979) Mössbauer analysis of iron-bearing phases in coal, coke, and ash. Analytical Methods for Coal and Coal Products, 3, 371–423.
Hyde, B.C., King, P.L., Dyar, M.D., Spilde, M.N., Ali, A.-M.S., and Kinkel, T. (2011) Methods to analyze metastable and microparticulate hydrated and hydrous iron sulfate minerals. American Mineralogist, 96, 1856–1869.
Johnston, J.H. (1977) Jarosite and akagenite from White Island Volcano, New Zealand—An X-ray and Mössbauer study. Geochimica et Cosmochimicia Acta, 41, 539–544.
Klingelhöfer, G., Morris, R.V., Bernhardt, B., Schröder, C., Rodionov, D.S., de-Souza, P.A., Yen, A., Gellert, R., Evlanov, E.N., Zubkov, B., and others. (2004) Jarosite and hematite at Meridiani Planum from Opportunities Mössbauer spectrometer. Science, 306, 1740–1745.
Kovács, K., Kuzmann, E., Homonnay, Z., Vértes, A., Gunneriusson, L., and Sandstron, A. (2008) Mössbauer study of synthetic jarosites. Hyperfine Interactions, 186, 69–73.
Lane, M.D., Dyar, M.D., and Bishop, J.L. (2004) Spectroscopic evidence for hydrous iron sulfate in the martian soil. Geophysical Research Letters, 31, L19702, doi: 10.1029/2004GL021231.
Leclerc, A. (1980) Room temperature Mössbauer analysis of jarosite-type compounds. Physics and Chemistry of Minerals, 6, 327–334.
Lin, J., Chen, N., Nilges, M.J., and Pan, Y. (2013) Arsenic speciation in synthetic gypsum ($CaSO_4{\cdot}2H_2O$): A synchrotron XAS, single-crystal EPR, and pulsed ENDOR study. Geochimica et Cosmochimica Acta, 106, 524–540.
Long, G.J., Longworth, G., Day, P., and Beveridge, D. (1980) A Mössbauer effect study of the electronic and magnetic properties of voltaite, a mixed-valence mineral. Inorganic Chemistry, 19, 821–829.
Lovas, G.A. (1986) Structural study of halotrichite from Recsk (Matra Mts., N. Hungary). Acta Geologica Hungarica, 29, 389–398.
Majzlan, J., Botez, C., and Stephens, P.W. (2005) The crystal structures of synthetic $Fe_2(SO_4)_3(H_2O)_5$ and the type specimen of lausenite. American Mineralogist, 90, 411–416.
Majzlan, J., Alpers, C.N., Bender Koch, C., McCleskey, R.B., Myneni, S.C.B., and Neil, J.M. (2011) Vibrational, X-ray absorption, and Mössbauer spectra of sulfate minerals from the weathered massive sulfide deposit at Iron Mountain, California. Chemical Geology, 284, 296–305.
Majzlan, J., Schlicht, H., Wierzbicka-Wieczorek, M., Giester, G., Pollman, H., Brömme, B., Doyle, S., Buth, S., and Bender Koch, C. (2013) A contribution to the crystal chemistry of the voltaite group: solid solutions, Mössbauer and infrared spectra, and anomalous anisotropy. Mineralogy and Petrology, 107, 221–233.
McAdam, A.C., Franz, H., Archer, P. Jr., Freissiner, C., Sutter, B., Glavin, D., Eigenbrode, J., Bower, H., Stern, J., Mahaffy, P.R., and others and the MSL Science Team (2013) Insights into the sulfur mineralogy of martian soil at Rocknest, Gale Crater, enabled by evolved gas analysis. Lunar and Planetary Science, Abstract 44, 1751.
Menchetti, S., and Sabelli, C. (1976) The halotrichite group: The crystal structure of apjohnite. Mineralogical Magazine, 40, 599–608.
Mereiter, K. (1972) Die kristallstruktur des voltaits, $K_2Fe^{2+}_3Fe^{3+}_3Al[SO_4]_{12}{\cdot}18H_2O$. Tschermaks Mineralogische und Petrographische Mitteilungen, 18, 185–202.
——— (1974) Die kristallstruktur von rhomboklas, $H_5O^+_2\{Fe[SO_4]_2{\cdot}2H_2O\}$. Tschermaks Mineralogische und Petrographische Mitteilungen, 21, 216–232.
Miyake, M., Minato, I., Morikawa, H., and Iwai, S.I. (1978) Crystal structure and sulphate force constants of barite, celestite, and anglesite. American Mineralogist, 63, 506–510.
Montano, P.A. (1981) Transformations and role of iron sulfides in coal liquefaction. Bulletin of the American Physical Society, 26, 201–201.
Moore, P.B. (1970) Structural hierarchies among minerals containing octahedrally coordinating oxygen. Neues Jahrbuch für Mineralogie Monatshefte, 163–173.
——— (1973) Bracelets and pinwheels—Topological geometrical approach to calcium orthosilicate and alkali sulfate structures. American Mineralogist, 58, 32–42.
Morris, R.V., Ming, D.W., Golden, D.C., and Bell, J.F. (1996) An occurrence of jarositic tephra on Mauna Kea, Hawaii; implications for the ferric mineralogy of the Martian surface. Mineral spectroscopy; a tribute to Roger G. Burns Special Publication—Geochemical Society, 5, 327–336.
Morris, R.V., Klingelhöfer, G., Bernhardt, B., Schröder, C., Rodionov, D.S., deSouza, P.A., Yen, A., Gellert, R., Evlanov, E.N., Foh, J., and others. (2004) Mineralogy at Gusev Crater from the Mossbauer spectrometer on the Spirit rover. Science, 305, 833–836.
Morris, R.V., Klingelhöfer, G., Schröder, C., Rodionov, D.S., Yen, A., Ming, D.W., de Souza, P.A. Jr., Wdowiak, T., Fleischer, I., Gllert, R., and others. (2006) Mössbauer mineralogy of rock, soil, and dust at Meridiani Planum, Mars: Opportunity's journey across sulfate-rich outcrop, basaltic sand and dust, and hematite lag deposits. Journal of Geophysical Research, 111, E12S15, doi:10.1029/2006JE002791.
Morris, R.V., Ming, D.W., Yen, A., Arvidson, R.E., Gruener, J., Humm, D., Klingelhöfer, G., Murchie, S., Schroder, C., Seelos, F. IV, Squyres, S., Wiseman, S., Wolff, M., and the MER and CRISM Science Teams (2007) Possible evidence for iron sulfate, iron sulfides, andelemental sulfur at Gusev Crater, Mars, from MER, CRISM, and analog data. 7th International Conference on Mars, Abstract 3393.
Morris, R.V., Klingelhöfer, G., Schröder, C., Fleischer, I., Ming, D.W., Yen, A.S., Gellert, R., Arvidson, R.E., Rodionov, D.S., Crumpler, L.S., Clark, B.C., and others. (2008) Iron mineralogy and aqueous alteration from Husband Hill through Home Plate at Gusev Crater, Mars: Results from the Mössbauer instrument on the Spirit Mars Exploration Rover. Journal of Geophysical Research, 113, E12S42, doi:10.1029/2008JE003201.
Musíc, S., Orehovec, Z., Popovic, S., and Czako-Nagy, I. (1994) Structural properties of precipitates formed by hydrolysis of Fe^{3+} ions in $Fe_2(SO_4)_3$ solutions. Journal of Materials Science, 29, 1991–1998.
Nomura, K., Takeda, M., Iiyama, T., and Sakai, H. (2005) Mössbauer studies of jarosite, mikasaite, and yavapaiite, and implication to their martian counterparts. Hyperfine Interactions, 166, 657–664.
Pankhurst, Q.A., McCann, V.H., and Newman, N.A. (1986) Identification of the iron-bearing minerals in some bituminous coals using Mössbauer spectroscopy. Fuel, 65, 880–883.
Parafiniuk, J., Bobrzycki, L., and Wozniak, K. (2010) Slavikite—revision of chemical composition and crystal structure. American Mineralogist, 95, 11–18.
Pax, R.A., and Clark, P.E. (1988) Application of Mössbauer spectroscopy to the coals of central Queensland. Hyperfine Interactions, 41, 839–842.
Peterson, R.C. (2003) The relationship between Cu content and distortion in the atomic structure of melanterite from the Richmond mine, Iron Mountain, California. The Canadian Mineralogist, 41, 937–949.
Peterson, R.C., Hammarstrom, J.M., and Seal, R.R. (2006) Alpersite (Mg,Cu) $SO_4{\cdot}7H_2O$, a new mineral of the melanterite group, and cuprian pentahydrite: Their occurrence within mine waste. American Mineralogist, 91, 261–269.
Reyes, F.A.G., Barraza, J.M., Bohorquez, A., Tabares, J.A., and Speziali, N.L. (2003) Mössbauer and XRD characterization of the mineral matter of coal from the Guachinte mine in Colombia. Hyperfine Interactions, 148, 39–46.
Ribeiro, F.R., Mussel, W.N., Fabris, J.D., Novais, R.F., and Garg, V.K. (2003) Identification of iron-bearing minerals in solid residues from industrial kaolin processing. Hyperfine Interactions, 148/149, 47–52.
Rieder, R., Gellert, R., Anderson, R.C., Brückner, J., Clark, B.C., Dreibus, G., Economou, T., Klingelhöfer, G., Lugmair, G.W., Ming, D.W., and others. (2004) Chemistry of rocks and soil at Meridiani Planus from the alpha particle X-ray spectrometer. Science, 306, 1746–1768.
Ristić, M., Musić, S., and Orehovec, Z. (2005) Thermal decomposition of synthetic ammonium jarosite. Journal of Molecular Structure, 744–747, 295–300.
Robinson, K., Gibbs, G.V., and Ribbe, P.H. (1971) Quadratic elongation: A quantitative measure of distortion in coordination polyhedra. Science, 172, 567–570.
Robinson, P.D., and Fang, J.H. (1971) Crystal structures and mineral chemistry of hydrated ferric sulphates: II. The crystal structure of paracoquimbite. American Mineralogist, 56, 1567–1572.
——— (1973) Crystal structures and mineral chemistry of hydrated ferric sulphates. III. The crystal structure of kornelite. American Mineralogist, 58, 535–539.
Rodríguez, N., Menéndez, N., Tornero, J., Amils, R., and de la Fuente, V. (2005) Internal iron biomineralization in Imperata cylindrical, a perennial grass: chemical composition, speciation and plant localization. New Phytologist, 165, 781–789.
Rothstein, Y. (2006) Spectroscopy of jarosite and implications for the mineralogy of Mars. B.A. thesis, Mount Holyoke College, South Hadley, Massachusetts.
Russell, P.E., and Montano, P.A. (1978) Erratum: Magnetic hyperfine parameters of iron containing minerals in coals. Journal of Applied Physics, 49, 4615–4617.
Sakai, N., Sekizawa, H., and Ono, K. (1981) Mössbauer spectroscopic identification of the gamma-ray radiolytic product of $FeSO_4{\cdot}7H_2O$ as $FeSO_4OH{\cdot}2H_2O$. Journal of Inorganic and Nuclear Chemistry, 43, 1731–1734.
Sallam, H.A., Eissa, N.A., Sheta, N.H., Soliman, M.A., and El-Fouly, M.H. (1994) Mössbauer effect, X-ray diffraction, and infrared studies of the effect of gamma irradiation on the molecular bonding of melanterite. Physics and Chemistry of Solids, 55, 1175–1180.
Schwertmann, U., Bigham, J.M., and Murad, E. (1995) The first occurrence of schwertmannite in a natural stream environment. European Journal of Min-

eralogy, 7, 547–552.
Scordari, F. (1975) The metavoltine problem: metavoltine from Madeni Zakh and Chuquicamata, and a related artificial compound. Minrralogical Magazine, 41, 371–374.
——— (1977) The crystal structure of ferrinatrite, $Na_3(H_2O)_3[Fe(SO4)_3]$ and its relationship to Maus's salt, $(H_3O)_2K_2\{K_{0.5}(H_2O)_{0.5}\}_6[Fe_3O(H_2O)_3(SO_4)_6](OH)_2$. Mineralogical Magazine, 41, 375–383.
——— (1981) Fibroferrite: A mineral with a $\{Fe(OH)(H_2O)_2SO_4\}$ spiral chain and its relationship to $Fe(OH)SO_4$, butlerite and parabutlerite. Tschermaks Mineralogische und Petrographische Mitteilungen, 28, 17–29.
Scordari, F., and Ventruti, G. (2009) Sideronatrite, $Na_2Fe(SO_4)_2(OH)\cdot 3H_2O$: Crystal structure of the orthorombic polytype and OD character analysis. American Mineralogist, 94, 1679–1686.
Scordari, F., Ventruti, G., and Gualtieri, A.F. (2004) The structure of metahohmannite, $Fe_2[O(SO_4)_2]$. $4H_2O$, by in situ synchrotron powder diffraction. American Mineralogist, 89, 365–370.
Segeler, C.G., Moore, P.B., Dyar, M.D., Leans, F., and Ferraiolo, J.A. (2012) Ferrolaueite, a new mineral from Monmouth County, New Jersey, U.S.A. Australian Journal of Mineralogy, 16, 69–76.
Sgarlata, F. (1985) The role of iron in halotrichite and in an osumilite. In Yu.M. Kagan and I.S. Lyubutin, Eds., Applications of the Mössbauer effect, 5, 1775–1778. Gordan and Breach Science Publishers.
Silva, L.F.O., Izquierdo, M., Querol, X., Finkelman, R.B., Oliveira, M.L.S., Wollenschlager, M., Towler, M., Pérez-López, R., and Macias, F. (2011) Leaching of potential hazardous elements of coal cleaning rejects. Environmental Monitoring Assessment, 175, 109–126.
Sklute, E.C. (2006) Mössbauer spectroscopy of synthetic olivine across the Fe-Mg solid solution. B.A. Thesis, Mount Holyoke College, South Hadley, Massachusetts.
Sklute, E.C., Y. Rothstein, M.W. Schaefer, O.N. Menzies, P.A. Bland, and F.J. Berry (2005) Temperature dependence and recoil-free fraction effects in olivines across the Mg-Fe solid solution. Lunar and Planetary Science Conference, 36, Abstract no.1888.
Stiller, A.H., Renton, J.J., Montano, P.A., and Russell, P.E. (1978) Application of Mössbauer spectroscopy to monitor acidmine drainage potentials of coal seams. Fuel, 57, 447–448.
Süsse, P. (1967) Die kristallstruktur des botryogens. Naturwissenschaften, 54, 139–139.
——— (1968a) Die kristallstruktur des botryogens. Acta Crystallographica, B24, 760–767.
——— (1968b) The crystal structure of amarantite, $Fe_2(SO_4)_2O\cdot 7H_2O$. Zeitschrift für Kristallographie, 127, 261–275.
Szymanski, J.T. (1988) The crystal structure of plumbojarosite $Pb(Fe,Al)_3((As,S)O_4)_2(OH)_2$. Canadian Mineralogist, 23, 659–668.
Takano, M., Shinio, T., Kiyama, M., and Takada, T. (1968) Magnetic properties of jarosites, $RFe_3(OH)_6(SO_4)_2$(R=NH_4, Na or K). Journal of Physical Science of Japan, 25, 902.
Taneja, S.P., and Jones, C.H.W. (1984) Magnetic hyperfine parameters of iron containing phases in coal and coal ash. Nuclear Physics and Solid State Physics Symposium, 26, 288–289.
Thomas, J.N., Robinson, P.D., and Fang, J.H. (1974) Crystal structures and mineral chemistry of hydrated ferric sulfates. IV. The crystal structure of quenstedtite. American Mineralogist, 59, 582–586.
Tosca, N.J., S.M. McLennan, D.H. Lindsley, and M.A.A. Schoonen (2004) Acid-sulfate weathering of synthetic martian basalt: The acid fog model revisited. Journal of Geophysical Research, 109, E05003, doi: 10.1029/2003JE002218.
Van Alboom, A., De Resende, V.G., De Grave, E., and Gomez, J.A.M. (2009) Hyperfine interactions in szomolnokite ($FeSO_4\cdot H_2O$). Journal of Molecular Structure, 924–926, 448–456.
van der Kraan, A.M., Niemantsverdriet, J.W., and Gerkema, E. (1984) Mössbauer spectroscopy used in energy studies. Energiespectrum, 84, 104–111.
Ventruti, G., Stasi, F., and Scordari, F. (2010) Metasideronatrite: crystal structure and its relation with sideronatrite. American Mineralogist, 85, 329–334.
Verma, H.C., and Tripathi, R.P. (2000) Characterization of iron-bearing minerals in Giril lignite from Rajasthan and study of their decomposition during combustion using Fe-57 Mössbauer spectroscopy. Fuel, 79, 599–606.
Waanders, F.B., Vinken, E., Mans, A., and Mulaba-Bafubiandi, A.F. (2003) Iron minerals in coal, weathered coal and coal ash—SEM and Mössbauer results. Hyperfine Interactions, 148, 21–29.
Wildner, M., and Giester, G. (1991) The crystal structures of kieserite-type compounds. I. Crystal structures of $Me(II)SO_4\cdot H_2O$ (Me = Mn,Fe,Co,Ni,Zn). Neues Jahrbuch für Mineralogie, Monatshefte, 296–306.
Yen, A.A., Gellert, R., Clark, B.C., Ming, D.W., King, P.L., Schmidt, M.E., Leshin, L., Morris, R.V., Squyres, S.W., Spray, J., Campbell, J.L., and the MSL Science Team (2013) Evidence for a global martian soil composition extends to Gale Crater. Lunar and Planetary Science Conference, 44, Abstract no. 2495.

Manuscript received May 14, 2013
Manuscript accepted July 25, 2013
Manuscript handled by Brian Phillips